Large Eddy Simulations of Flow Around Two Circular Cylinders in Tandem in the Vicinity of a Plane Wall at Small Gap Ratios

Zhong Li^{a,*}, Mia Abrahamsen Prsic^c, Muk Chen Ong^b,
Boo Cheong Khoo^d

^{a} *NUS Graduate School for Integrative Sciences and Engineering, National University of Singapore, Singapore*

^{b} *Department of Mechanical and Structural Engineering and Materials Science, University of Stavanger, Norway*

^{c} *Department of Marine Technology, Norwegian University of Science and Technology, Norway*

^{d} *Department of Mechanical Engineering, National University of Singapore, Singapore*

Abstract

Large Eddy Simulations (LES) with Smagorinsky subgrid scale model have been performed for the flow past two circular cylinders in tandem placed in the vicinity of a horizontal plane wall at very small gap ratios, namely $G/D = 0.1, 0.3$ and 0.5, in three-dimension (3D). The ratio of cylinder center-to-center distance to cylinder diameter, or the pitch ratio, L/D, considered in the simulations is $L/D = 2$ and 5. This work serves as an extension of Abrahamsen Prsic et al. (2015) [1]. In essence, six sets of simulations have been performed in the subcritical Reynolds number regime at $Re = 1.31 \times 10^4$. Our major findings can be summarized as follows. (1) At both pitch ratios, the wall proximity has a decreasing effect on the mean drag coefficient of the upstream cylinder. At $L/D = 2$, the mean drag coefficient of the downstream cylinder is negative since it is located within the drag inversion separation distance. (2) At $L/D = 2$, a squarish cavity-like flow exists between the cylinders and the flow circulates within the cavity. A long lee-wake recirculation zone is found behind the downstream cylinder at $G/D = 0.1$. However, a much smaller lee-wake recirculation zone is noticed at $L/D = 5$ with $G/D = 0.1$. (3) At $L/D = 2$, the reattachment is biased to the bottom shear layer due to the deflection from the plane wall, which leads to the formation of the slanted squarish cavity-like flow. At both pitch ratios, as G/D becomes smaller, stronger vortices are found between the two cylinders. Vortices of less intensity are observed in the near wake of the downstream cylinder due to the vortex shedding suppression of the neighbouring wall.

Key Words: tandem circular cylinders, wall proximity, flow interference, Large Eddy Simulations (LES), flow structures

1 INTRODUCTION

Circular cylinders in an isolated configuration or in bundles are commonly seen in the offshore and ocean engineering structures. Subsea pipelines, marine risers and columns of semi-submersibles are salient examples. Owing to the practical significance in engineering applications, flow past an isolated circular cylinder is well documented in the open literature. Zdravkovich (1997) [2] as well as Sumer and Fredsøe (2010) [3] gave comprehensive reviews on flow around an isolated single cylinder. Experimental studies on this topic can date back to Thom (1928) [4] where an investigation of the fluid flow around a cylinder was conducted almost a century ago. In recent years, modern particle image velocimetry (PIV) measurements have been employed in the flow visualization. Parnaudeau et al. (2008) [5] utilized PIV to investigate flow over a circular cylinder at $Re = 3.9 \times 10^3$. With regard to recent computational fluid dynamics (CFD) studies, Lysenko et al. (2012) [6] and Abrahamsen Prsic et al. (2014) [7] performed LES of the flow past a circular cylinder at $Re = 3.9 \times 10^3$ and at 1.31×10^4 ($Re \equiv U_\infty D/\nu$ where U_∞ is the free stream velocity, D is the cylinder diameter, and ν is the kinematic viscosity of the fluid), respectively, using the Open Source Field Operation and Manipulation (OpenFOAM) code.

In real ocean engineering applications, offshore structures in the form of circular cylinders frequently appear in pairs. The effect of the presence of other bodies in the flow is called the flow interference, one type of which being wake interference. The wake interference happens when a body is placed behind another in relation to the free stream. In such a situation, the flow impinging on the downstream body is strongly altered. In the simplest possible scenario, two cylinders of identical diameter in tandem arrangement are subjected to incoming steady currents. The flow behaviour in this case becomes complex due to the interaction of the vortex streets of the upstream cylinder with the shear layer of the downstream cylinder and the interaction between the vortices shed from both cylinders. Besides Re, the ratio of center-to-center distance to cylinder diameter, L/D, is another governing parameter as the presence of the downstream cylinder has a dramatic influence on the flow behaviour around both cylinders. Two representative works on flow classification were presented by Zdravkovich (1985, 1987) [8] [9]. In these works, three main regimes were identified, namely the extended-body, the reattachment and the co-shedding regimes. Generally, a large L/D in the co-shedding regime allows vortex shed-

---

* Corresponding author
  Email address: `lizhong@u.nus.edu` (Zhong Li).

2

ding from both cylinders, while a smaller L/D in the other two regimes suppresses the vortex shedding from the upstream one. In the extended-body regime, the downstream cylinder is located inside the vortex formation region of the upstream cylinder and the separated shear layers from the upstream cylinder are forced to wrap around the downstream cylinder prior to rolling up alternatingly into Kármán vortices behind the downstream cylinder. In the reattachment regime, the shear layers from the upstream cylinder no longer enclose the downstream cylinder but rather attach onto the downstream cylinder. In the co-shedding regime, the downstream cylinder is sufficiently far away from the upstream cylinder so that Kármán vortices form from both cylinders. The downstream cylinder, located outside the vortex formation region of the upstream cylinder, experiences the periodic impingement of the vortices shed from the upstream cylinder. Other pioneering works on the classification of the flow past two tandem cylinders depending on Re and L/D include Igarashi (1981, 1984) [10, 11], Xu and Zhou (2004) [12] and Zhou and Yiu (2006) [13].

A number of experimental studies carried out to investigate the flow around two cylinders in tandem can be found in Zdravkovich and Pridden (1977) [14], Lin et al. (2002) [15], Alam et al. (2003) [16], Zhou and Yiu (2006) [13] and Song et al. (2015) [17]. Most of the experiments were performed in the subcritical Re regime ranging from 10^4 to 8×10^4. Sumner (2010) [18] gave a detailed review of the experimental studies for two cylinders in tandem. As for the numerical studies of the flow around wall-free tandem cylinders, many of the works are limited to two-dimensional (2D) simulations at low Re. Mittal et al. (1997) [19] employed a finite element formulation to investigate flow past a pair of cylinders in tandem at $Re = 100$ and 1000. Meneghini et al. (2001) [20] used a fractional step method to study the vortex shedding and flow interference between two cylinders in tandem at Re from 100 to 200. Carmo et al. (2010) [21] employed a high-order spectral element method and performed direct stability analysis to characterize secondary instabilities in the wake of the flow past two cylinders in tandem arrangements, with L/D ranging from 1.2 to 10 in the low Re regime. They identified three regimes based on the vortex shedding in the gap between the two cylinders, namely SG (symmetric in the gap), AG (alternating in the gap) and WG (wake in the gap). Numerical simulations for high Re regime in recent years include Kitagawa and Ohta (2008) [22], Uzun and Hussaini (2012) [23] and Gopalan and Jaiman (2015) [24]. In Kitagawa and Ohta (2008) [22], standard LES were utilized to perform 3D studies on flow around two tandem cylinders with L/D ranging from 2 to 5 at $Re = 2.2 \times 10^4$. Uzun and Hussaini (2012) [23] employed the delayed detached eddy simulations (DDES) to investigate the flow past two tandem cylinders with $L/D = 3.7$ at $Re = 1.66 \times 10^5$. Gopalan and Jaiman (2015) [24] employed a hybrid unsteady Reynolds-averaged Navier-Stokes (URANS) - LES model to study the flow interference between tandem cylinders with $L/D = 1.4$, 3.0 and 3.7 at $Re = 1.66 \times 10^5$.

When the cylinder is placed near a plane boundary, the proximity of a plane wall introduces complexities to the vortex shedding in the wake. In this case, two important parameters are the ratio of gap between the cylinder and wall to diameter, G/D, and the ratio of boundary layer thickness to diameter, δ/D. One of the earliest experiments studying ground effect on a circular cylinder was reported by Taneda (1965) [25], where the flow behind a circular cylinder towed through stagnant water close to a fixed ground was visualised at $Re = 170$. The water and ground moved together relative to the cylinder and thus there was essentially no boundary layer formed on the ground. Regular alternate vortex shedding occurred at a gap ratio $G/D = 0.6$, while only a weak single row of vortices were shed at $G/D = 0.1$.

There are relatively limited works concerning the studies on flow around near-wall tandem cylinders. Bhattacharyya and Dhinakaran (2008) [26] and Harichandan and Roy (2012) [27] presented numerical simulations at low Re of 100 and 200. Rao et al. (2013) [28] conducted numerical investigations on the dynamics and stability of the flow past two tandem cylinders sliding along a wall for $20 \leq Re \leq 200$. Wang et al. (2015) [29] measured the flow past two cylinders in tandem at G/D between 0.15 and 2.0 and L/D ranging from 1.5 to 6 at $Re = 6.3 \times 10^3$. Abrahamsen Prsic et al. (2015) [1] performed LES for flow around tandem cylinders in the vicinity of a plane wall with $G/D = 1$ and $L/D = 2$ and 5 at $Re = 1.31 \times 10^4$. In D'Souza et al. (2016) [30], the dynamics and the wake stability were studied for the flow past tandem cylinders in proximity to a plane moving wall at $Re = 200$.

To the best of our knowledge, there are very few numerical studies on flow around near-wall tandem cylinders, particularly at very small gap ratios. This work serves as one step forward to understanding the flow physics involved in the flow past two cylinders in tandem placed in close proximity to a wall. This set-up often appears in double free-spanning subsea pipelines which are frequently seen in offshore applications. LES for the flow around two near-wall tandem cylinders with $L/D = 2$ and 5 and G/D ranging from 0.1 to 0.5 at $Re = 1.31 \times 10^4$ in the subcritical regime will be presented in this work. The presentation of the results will be primarily on three aspects: (1) hydrodynamic force coefficients; (2) time-averaged flow characteristics; and (3) instantaneous flow fields.

The remainder of this article is organized as follows. In Section 2, the mathematical formulation is described. The numerical problem description is defined in Section 3. This is followed by the LES results and discussions in Section 4. Finally, the concluding remarks are given in Section 5.

2 Numerical Methodology

In the present study, LES are performed with the Smagorinsky subgrid-scale model. The incompressible Navier-Stokes equations in the filtered form can be written as

$$\frac{\partial \overline{u}_i}{\partial x_i} = 0 \tag{1}$$

$$\frac{\partial \overline{u}_i}{\partial t} + \frac{\partial (\overline{u}_i \overline{u}_j)}{\partial x_j} = -\frac{1}{\rho}\frac{\partial \overline{p}}{\partial x_i} + \nu \frac{\partial^2 \overline{u}_i}{\partial x_j^2} - \frac{\partial \tau_{ij}}{\partial x_j} \tag{2}$$

where $\overline{u}_i$ ($i \in [1, 2, 3]$) denotes the filtered velocity component in streamwise (x), crossflow (y) and spanwise (z) directions, respectively. ρ is the density of the fluid, $\overline{p}$ is the filtered pressure, and τ is the non-resolvable subgrid stress, which is given by the following,

$$\tau_{ij} = \overline{u_i u_j} - \overline{u}_i \overline{u}_j. \tag{3}$$

The widely used subgrid scale model originally proposed by Smagorinsky (1963) [31] is used here to take the subgrid motions into account. By Boussinesq approximation, introducing the turbulent eddy viscosity ν_t yields the following expression for the subgrid stress,

$$\tau_{ij} - \frac{1}{3}\delta_{ij}\tau_{kk} = -2\nu_t \overline{S}_{ij}. \tag{4}$$

Here, $\overline{S}_{ij} = \frac{1}{2}(\frac{\partial \overline{u}_i}{\partial x_j} + \frac{\partial \overline{u}_j}{\partial x_i})$ denotes the strain rate tensor in the resolved field and δ_{ij} is the Kronecker delta. ν_t is a function of $\overline{S}_{ij}$ and the subgrid length l, and given as

$$\nu_t = l^2 \mid \overline{S}_{ij} \mid . \tag{5}$$

The subgrid length l is given by

$$l = C_s \overline{\Delta} \tag{6}$$

where C_s is the Smagorinsky constant, set at 0.2, and Δ denotes the grid filter width. The standard Smagorinsky model was successfully applied in the cases

of flow over a single cylinder and tandem cylinders in proximity to a plane wall in Abrahamsen Prsic et al. (2016, 2015) [1, 32], respectively. Therefore, the standard Smagorinsky model is chosen over other subgrid scale models in this study.

The instantaneous lift and drag coefficients are defined as

$$C_L = \frac{F_y}{\frac{1}{2}\rho U_\infty^2 DS}, \qquad C_D = \frac{F_x}{\frac{1}{2}\rho U_\infty^2 DS} \qquad (7)$$

where the fluid loading F_y and F_x represent the lift and drag, respectively, and S is the spanwise length of the cylinder.

All simulations are performed using the OpenFOAM C++ code. The PISO (Pressure Implicit with Splitting of Operators) algorithm is employed to solve the Navier-Stokes equations, see Ferziger and Peric (2001) [33]. As for the time integration, the implicit second-order Crank-Nicolson scheme is used. The numerical methodology has been validated using the benchmark test of the flow around an isolated circular cylinder and a circular cylinder placed in the vicinity of a plane wall in Abrahamsen Prsic et al. (2014, 2016) [7, 32] at the same Re as in the present study, respectively. The results were compared well with published experimental and numerical data published previously, so the LES model implemented in the OpenFOAM code is deemed adequate for this study.

3   Problem Description

3.1   Computational Set-up

The schematic diagram is shown in Figure 1. The length, width and height of the 3D computation domain are $40D + L$, $4D$ and $11.5D$, respectively. This ensures that the top boundary has no effect on the flow around the cylinder and the bottom wall. The upstream cylinder is placed at the upstream distance of $L_U = 10D$ from the inlet and the downstream cylinder is located at the upstream distance of $L_D = 30D$ from the outlet. These distances are sufficient to eliminate the far field effects from the flow upstream and downstream of the cylinders. The center-to-center distance between the tandem cylinders is denoted by L. The gap between the cylinder and the bottom wall is represented by G. The same dimension of the 3D rectangular domain was also used in Abrahamsen Prsic et al. (2015) [1].

At the inlet, the incoming flow takes on a logarithmic velocity profile as in a

boundary layer flow, with the maximum streamwise velocity of U_∞. Natural boundary condition for the pressure is defined at the inlet. At the outlet, natural boundary condition for the velocity is applied, and the pressure is set to zero as the reference. No slip boundary conditions are applied on both the cylinders and the bottom wall, and free slip boundary condition is applied on the top boundary. Periodic boundary conditions are defined on the boundaries with two ends of the cylinder.
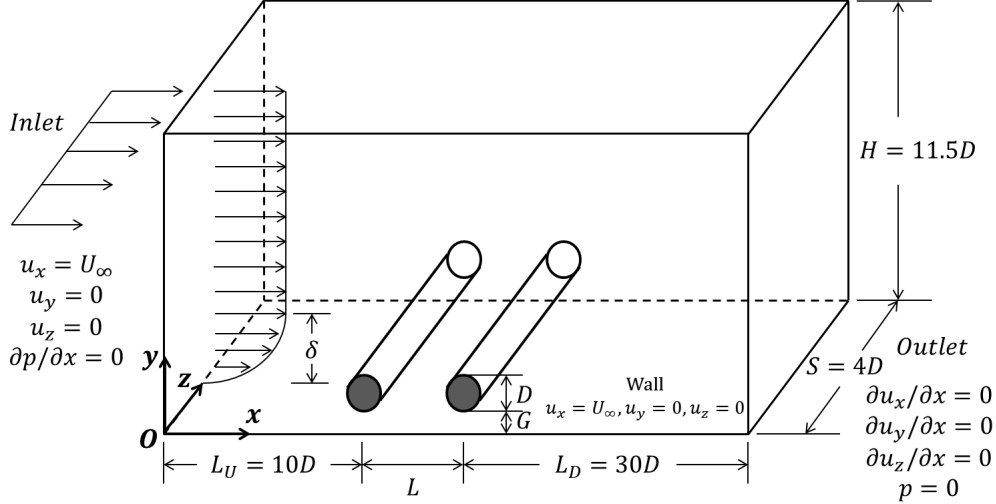

Figure 1. The schematic diagram of flow past near-wall tandem cylinders.

To eliminate the effect of the wall boundary layer thickness, the ratio of boundary layer thickness to the cylinder diameter, δ/D, is fixed at 0.48 throughout this study. According to Abrahamsen Prsic et al. (2016) [32], to mimic a fully developed boundary layer profile which free spanning pipelines placed close to the seabed frequently encountered in the actual subsea environment, a logarithmic velocity profile is imposed at the inlet. Further, $\delta/D = 0.48 - 0.50$ was also applied in previous experimental studies, see Lei et al. (1999) [34] and Wang et al. (2015) [29]. Therefore, $\delta/D = 0.48$ is kept constant throughout the present study. The vertically dependant streamwise velocity $u(y)$ is defined as in the following,

$$u(y) = min\left\{\frac{u_*}{k}ln(\frac{y}{z_w}), U_\infty\right\} \tag{8}$$

where $\kappa = 0.41$ is the von Kármán constant, $z_w = 10^{-6}m$ is the roughness of the bottom wall, and u_* denotes the friction velocity, evaluated by the following equation,

$$u_* = \frac{\kappa U_\infty}{ln(\delta/z_w)}. \tag{9}$$

The details of the boundary conditions and logarithmic wall functions applied

7

in this study can be referred to Ong et al. (2010) [35].

The ratio of center-to-center distance to cylinder diameter, or pitch ratio, L/D, is set at 2 and 5, to investigate expected reattachment and co-shedding regimes, respectively; and the gap ratio, G/D, is set at 0.1, 0.3 and 0.5. Therefore, six combinations of parameters in total are chosen to study the effects of L/D and G/D on the flow structures and the hydrodynamic forces acting on the cylinders.

3.2   Mesh

The case with $L/D = 2$ and $G/D = 0.3$ is taken as an example to illustrate the mesh utilized in the numerical simulations, as shown in Figure 2a. A body-fitted, structured mesh is divided into several zones to maintain the control over the element size in the vicinity of the cylinders and the bottom wall. As shown in Figure 2b, very fine elements are used close to the cylinders and between the cylinders in order to fully capture the dynamics of the cylinder wall boundary layer and the gap flow between the two cylinders. To be specific, the normalized radial distances from the cylinder wall, $(h_p)_c/D$, and the bottom wall, $(h_p)_w/D$, to the first nodes are approximately 7.0×10^{-3} and 1.2×10^{-3}, respectively. Figure 2c shows that the fine elements are also placed in the vicinity of the plane wall to capture the bottom wall boundary layer dynamics.

The 3D mesh is generated by layering the 2D mesh along the spanwise direction (z-axis). Following Abrahamsen Prsic et al. (2015) [1], a fine spanwise resolution of $\Delta z'/D = 0.04$ or 100 layers of mesh are used to discretize along the spanwise length of $4D$. The total number of elements of the mesh utilized in each case ranges from 20 to 25 million, as summarized in Table 1. The grid convergence and time-step convergence studies were systematically carried out in Abrahamsen Prsic et al. (2015) [1] for the flow around tandem cylinders placed at $L/D = 5$ and $G/D = 1$. For completeness, the grid and time-step convergence studies are tabulated in Tables 2 and 3. Following this reference, similar mesh densities are used in the present study. In Table 3, an engineering approach for the time-step convergence has been carried out to achieve the optimization between the numiercla accuracy and the efficiency due to the high computational cost for 3D turbulence simulations. The mean drag coefficient $\overline{C_D}$ of the upstream cylinder seems to fluctuate within a narrow range of approximately 5%. By reducing $\Delta t U_\infty/D$ by 50% from $T1$ to $T2$, $\overline{C_D}$ varies merely by 2.9%. Furhter reducing $\Delta t U_\infty/D$ by 60.3% from $T2$ to $T3$, $\overline{C_D}$ then varies by a mere 5.3%. Thus, the variation of $\overline{C_D}$ is acceptable considering the large extent of change in $\Delta t U_\infty/D$. By following the same reference, therefore, the same dimensionless time step, $U_\infty \Delta t/D = 1.31 \times 10^{-4}$, is used.
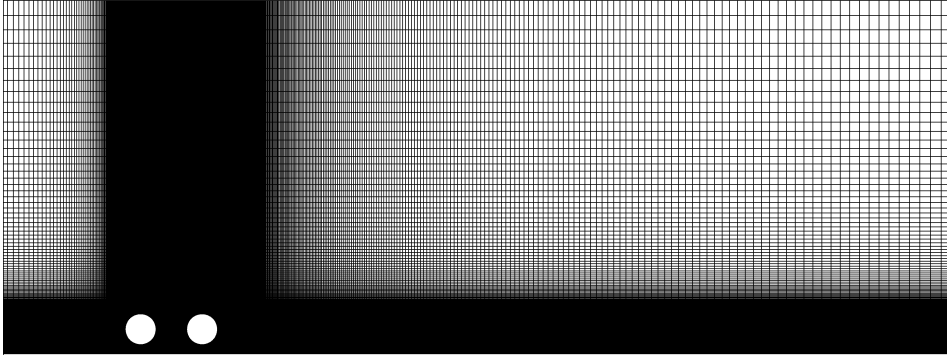
(a)
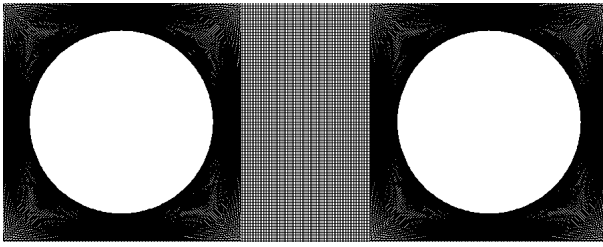
(b)
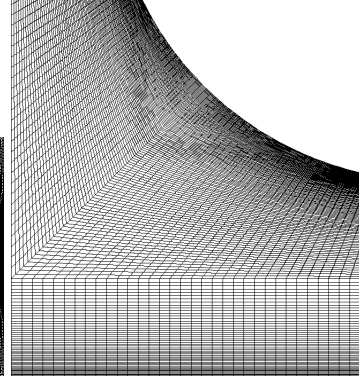
(c)

Figure 2. The mesh structure used in the case of $L/D = 2$ and $G/D = 0.3$: (a) Overall view, (b) Zoom-in view of tandem cylinders, and (c) Zoom-in view of a quadrant of the upstream cylinder and the neighbouring plane wall.

Table 1
Summary of mesh used in each simulation case

L/D	G/D	Hexahedra	Quadrangles	Total (approx.)
2	0.5	19.84×10^6	939×10^3	20.78×10^6
2	0.3	19.84×10^6	939×10^3	20.78×10^6
2	0.1	19.20×10^6	920×10^3	20.12×10^6
5	0.5	22.36×10^6	$1,037 \times 10^3$	23.40×10^6
5	0.3	22.36×10^6	$1,037 \times 10^3$	23.40×10^6
5	0.1	19.20×10^6	920×10^3	20.12×10^6

Figure 3 presents the energy spectra in the wake of the upstream cylinder

Table 2
Grid convergence study for $L/D = 5$ and $G/D = 1.0$ with $\Delta t U_\infty/D = 0.0013$, taken from Abrahamsen Prsic et al. (2015) [1]

Case	Number of Elements	$\overline{C_D}$ of Upstream Cylinder
$M1$	16.5×10^6	1.41
$M2$	21.0×10^6	1.39
$M3$	25.0×10^6	1.39

Table 3
Time-step convergence study for $L/D = 5$ and $G/D = 1.0$ with approximately 25 million elements, taken from Abrahamsen Prsic et al. (2015) [1]

Case	$\Delta t U_\infty/D$	$\overline{C_D}$ of Upstream Cylinder
$T1$	0.0006500	1.36
$T2$	0.0003275	1.32
$T3$	0.0001300	1.39

for the two cases with $G/D = 0.5$ at $L/D = 2$ and $L/D = 5$. Probes with the coordinates of $(11D, 1D, 2D)$ and $(12.5D, 1D, 2D)$ are located at the mid-point between the tandem cylinders for the two cases, respectively. Here, the specific kinetic energy, or kinetic energy per unit mass, E, is defined as $E = \frac{1}{2}[(u_x)^2 + (u_y)^2 + (u_z)^2]$ where u_x, u_y and u_z denote the instantaneous velocities at the probe locations in the streamwise, crossflow and spanwise directions, respectively. A fast Fourier transform (FFT) is performed on the specific kinetic energy measured.

The energy spectrum of the upstream cylinder wake at $G/D = 0.5$ and $L/D = 5$ shows that the energy reaches a maximum at $St = 0.21$ in the anisotropic range, indicating the presence of the periodic vortex shedding. This is in good agreement with the experiments of Wang et al. (2015) [29] reporting energy is maximum at $St = 0.19$. As shown in both cases, the normalized kinetic energy follows well with a $-5/3$ slope, the Kolmogorov spectrum, in the inertial subrange (see Kravchenko and Moin (2000) [36] and Mathieu and Scott (2000) [37]). It can be, therefore, concluded that the present simulations are capable of capturing the "$-5/3$ behaviour", implying the validity of the turbulence modelling in this study.

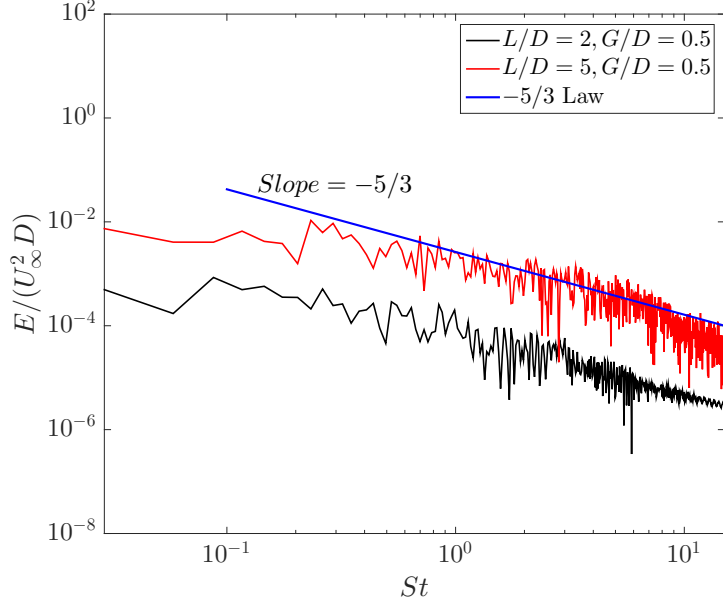The distance from the wall, i.e. cylinder walls and bottom plane wall, measured

Figure 3. Energy spectra of the probes located at the mid-point between tandem cylinders with $G/D = 0.5$ for both pitch ratios of $L/D = 2$ and 5. The y-axis represents the normalized specific kinetic energy and the x-axis is the Strouhal frequency, $St = fD/U_\infty$.

in viscous lengths is denoted by

$$y^+ = \frac{u_* \Delta y}{\nu}, \tag{10}$$

where Δy is the distance measured from the wall. It is critical to maintain $y^+|_{\Delta y = h_p} \leq 1$ when employing LES where h_p is the radial distance from the wall to the first node away from the wall, see Pope (2000) [38]. The values of average y^+ at the first node away from both the cylinder walls and the bottom plane wall for the two above-mentioned cases are tabulated in Table 4. For brevity, six time instances in the dimensionless time range of $tU_\infty/D \in [117.90, 131.00]$ (or dimensional time $t \in [90, 100]$) are taken for the purpose of illustration. It is seen in Table 4 that y^+ at the first node away from the wall is well maintained ($y^+ < 1$) as sufficiently fine grids are used around the cylinder walls and bottom wall, demonstrating the validity of LES used in this study.

11

Table 4
Summary of average $y^+|_{\Delta y=h_p}$ at the cylinder walls and bottom

Case	$L/D = 2, G/D = 0.5$			$L/D = 5, G/D = 0.5$		
tU_∞/D	Upstream cylinder	Downstream cylinder	Bottom	Upstream cylinder	Downstream cylinder	Bottom
117.90	0.379431	0.423216	0.352491	0.363316	0.420493	0.354880
120.52	0.342703	0.381334	0.421121	0.361386	0.427703	0.364518
123.14	0.382049	0.412782	0.340022	0.362267	0.393300	0.356924
125.76	0.383720	0.415006	0.323264	0.362710	0.352282	0.345955
128.38	0.383974	0.424450	0.321631	0.363503	0.355461	0.346791
131.00	0.383108	0.420575	0.308605	0.362175	0.344964	0.349590

4 Results & Discussion

4.1 Hydrodynamic Force Coefficients

The influence of the gap ratio, G/D, and the pitch ratio, L/D, on the hydrodynamic forces acting on the two cylinders in tandem placed close to a plane wall is investigated through the coefficients of mean lift $\overline{C_L}$ and mean drag $\overline{C_D}$, evaluated as

$$\overline{C_L} = \frac{1}{n} \sum_{i=1}^{i=n} C_{L,i}, \qquad \overline{C_D} = \frac{1}{n} \sum_{i=1}^{i=n} C_{D,i}, \qquad (11)$$

whereby their root-mean-square (RMS) counterparts are

$$(C_L)_{rms} = \sqrt{\frac{1}{n} \sum_{i=1}^{i=n} (C_{L,i} - \overline{C_L})^2}, \qquad (C_D)_{rms} = \sqrt{\frac{1}{n} \sum_{i=1}^{i=n} (C_{D,i} - \overline{C_D})^2}, \quad (12)$$

where n denotes the number of samples taken.

Note that the mean value is subtracted in computing the RMS quantities so that the $(C_L)_{rms}$ and $(C_D)_{rms}$ are direct indicators to measure the fluctuating amplitudes of C_L and C_D, respectively, without being affected by their non-zero mean values.

In the following, for simplicity, the subscript 1 denotes the upstream cylinder, and the subscript 2 denotes the downstream cylinder. The time histories of C_D and C_L of both the upstream and the downstream cylinders for the di-

mensionless time range $tU_\infty/D = 80 - 120$ after reaching quasi-steady state for all six simulated cases are shown in Figure 4. $C_{D,1}$ and $C_{L,1}$ denote the drag and lift coefficients for the upstream cylinder, respectively; and $C_{D,2}$ and $C_{L,2}$ denote the drag and lift coefficients for the downstream cylinder, respectively. It is noticeable that in all cases the fluctuation amplitudes of the forces acting on the downstream cylinder are remarkably larger than what is experienced by the upstream cylinder. This is owing to the fact that the downstream cylinder is subjected to the wake interference by the upstream cylinder. At all gap ratios, for $L/D = 5$, the fluctuation amplitudes of $C_{D,1}$ and $C_{L,1}$ are smaller than those of $L/D = 2$, which means that the downstream cylinder at $L/D = 2$ has a de-stablizing effect on its upstream counterpart in terms of the hydrodynamic forces.

It is worth noting that $C_{D,2}$ for $L/D = 2$ at all gap ratios considered stays in the negative range except for some moments of peaks, and is considerably lower than $C_{D,1}$. This can be understood when we note that at $L/D = 2$, the downstream cylinder is located inside the near wake behind the upstream cylinder and therefore in a low pressure region, which will be discussed later in Section 4.2.1 in detail. In such a case, the drag exerted on the downstream cylinder is usually negative, which is generally termed as the *drag inversion*. The phenomenon of drag inversion is also captured in the LES results reported by Kitagawa and Ohta (2008) [22] and Sainte-Rose et al. (2014) [39] for flow past wall-free tandem cylinders. One of the most important features reported in the earlier works is the discontinuity in the value of hydrodynamic forces when the pitch ratio is varied continuously. The spacing for which this discontinuity occurs is named *critical spacing* or *critical separation* and evidently depends on Re. It is also frequently referred to as the *drag inversion separation* since the drag on the downstream cylinder is negative in relation to the free stream direction for spacing smaller than the critical separation and positive for spacing larger than the critical separation. Therefore, in this context of flow past two near-wall tandem cylinders, from the observation of $C_{D,2}$, the critical drag inversion separation is between $2D$ and $5D$. However, finding the exact critical drag inversion separation at $Re = 1.31 \times 10^4$ in the near-wall configuration is not the focus of this study.

With the decrease in the gap ratio, the vortex shedding becomes more suppressed, which is evidenced by the fact that the fluctuation amplitude of C_L for both cylinders decreases. For instance, at $L/D = 2$ shown by Figures 4a, 4c and 4e, the time traces of $C_{L,1}$ and $C_{L,2}$ become more flattened with the decreasing G/D from 0.5 to 0.1. Ong et al. (2010) [35] pointed out that at small gap ratios the strong gap flow between the cylinder and the plane wall in proximity weakens the interaction between the two shear layers shed from the cylinder. The greater details of the vortex shedding will be further described in Section 4.2.2. There exists a critical gap ratio, $(G/D)_{crit}$, which can be defined as a gap ratio below which the vortex becomes suppressed. Based on the ex-

periments of Bearman and Zdravkovich (1978) [40], $(G/D)_{crit}$ was determined in the range from 0.3 to 0.4 at $Re = 4.5 \times 10^4$. Lei et al. (1999) [34] identified $(G/D)_{crit}$ to be from 0.2 to 0.3 at $Re = 1.3 - 1.45 \times 10^4$. Although finding the exact $(G/D)_{crit}$ is not the focus of this study, it can be determined here that the $(G/D)_{crit}$ of the upstream cylinder at $L/D = 2$ appears between 0.1 and 0.3. Zdravkovich (2009) [41] summarized that the wall proximity maintains a strong influence when G/D is small, leading to the complete disappearance of vortex shedding for the narrowest gaps. As G/D exceeds 1, the influence becomes insignificant. It is also noted that, at both pitch ratios, $\overline{C_{D,1}}$ is slightly above 1 at $G/D = 0.5$, approaching the value of $\overline{C_D}$ for an isolated cylinder in the subcritical regime, as documented in Sumer and Fredsøe (2010) [3].

The mean and RMS force coefficients of both the upstream and the downstream cylinders are calculated for the quasi-steady state. Figure 5 presents $\overline{C_D}$ and $\overline{C_L}$ of both cylinders with $L/D = 2$ and 5 as a function of G/D. Some other published experimental and numerical data for a single cylinder placed near a plane wall are included with the present results for comparison. $\overline{C_{D,1}}$ and $\overline{C_{L,1}}$ at $L/D = 2$ and 5 agree quite well with the reference data. As shown in Figure 5a, $\overline{C_{D,1}}$ decreases with the decrease in G/D, which is consistent with the conclusion drawn in other studies. Lei et al. (1999) [34] and Ong et al. (2012) [42] both reported the neighbouring wall has a decreasing effect on the mean drag. In other words, $\overline{C_{D,1}}$ decreases with the decrease in the gap ratio.

As for the downstream cylinder, $\overline{C_{D,2}}$ is considerably smaller than that of the upstream cylinder. For $L/D = 2$, which is within the critical drag inversion separation, as discussed earlier, $\overline{C_{D,2}} < 0$ for all cases of G/D. However, for $L/D = 5$, which is greater than the critical drag inversion separation, $\overline{C_{D,2}}$ is still negative at $G/D = 0.1$ and increases to the positive range with the increase of G/D. In Figure 5b, $\overline{C_{L,2}}$ shows different trends for different L/D. At $L/D = 2$, $\overline{C_{L,2}}$ stays in the positive range and increases with the increase of G/D. In contrast, at $L/D = 5$, $\overline{C_{L,2}}$ stays in the negative range and decreases with the increase of G/D. The reason for this is the skewness of the pressure distribution around the downstream cylinder which will be discussed in Section 4.2.1.

The RMS force coefficients $(C_D)_{rms}$ and $(C_L)_{rms}$ of both cylinders with $L/D = 2$ and 5 as a function of G/D are shown in Figure 6. As observed in Figure 6a, for both $L/D = 2$ and 5, $(C_{D,2})_{rms}$ increases with the increase of G/D and $(C_{D,1})_{rms}$ are close in value at different G/D. In Figure 6b, similarly with $(C_{D,2})_{rms}$, for both $L/D = 2$ and 5, $(C_{L,2})_{rms}$ increases with the increase of G/D due to the fact that the vortex shedding is more suppressed at a smaller G/D which leads to a smaller fluctuation amplitude of the lift coefficient. For the upstream cylinder, $(C_{L,1})_{rms}$ are quite close for different pitch ratios. It is shown that $(C_{D,2})_{rms}$ and $(C_{L,2})_{rms}$ agree quite well with the experimental
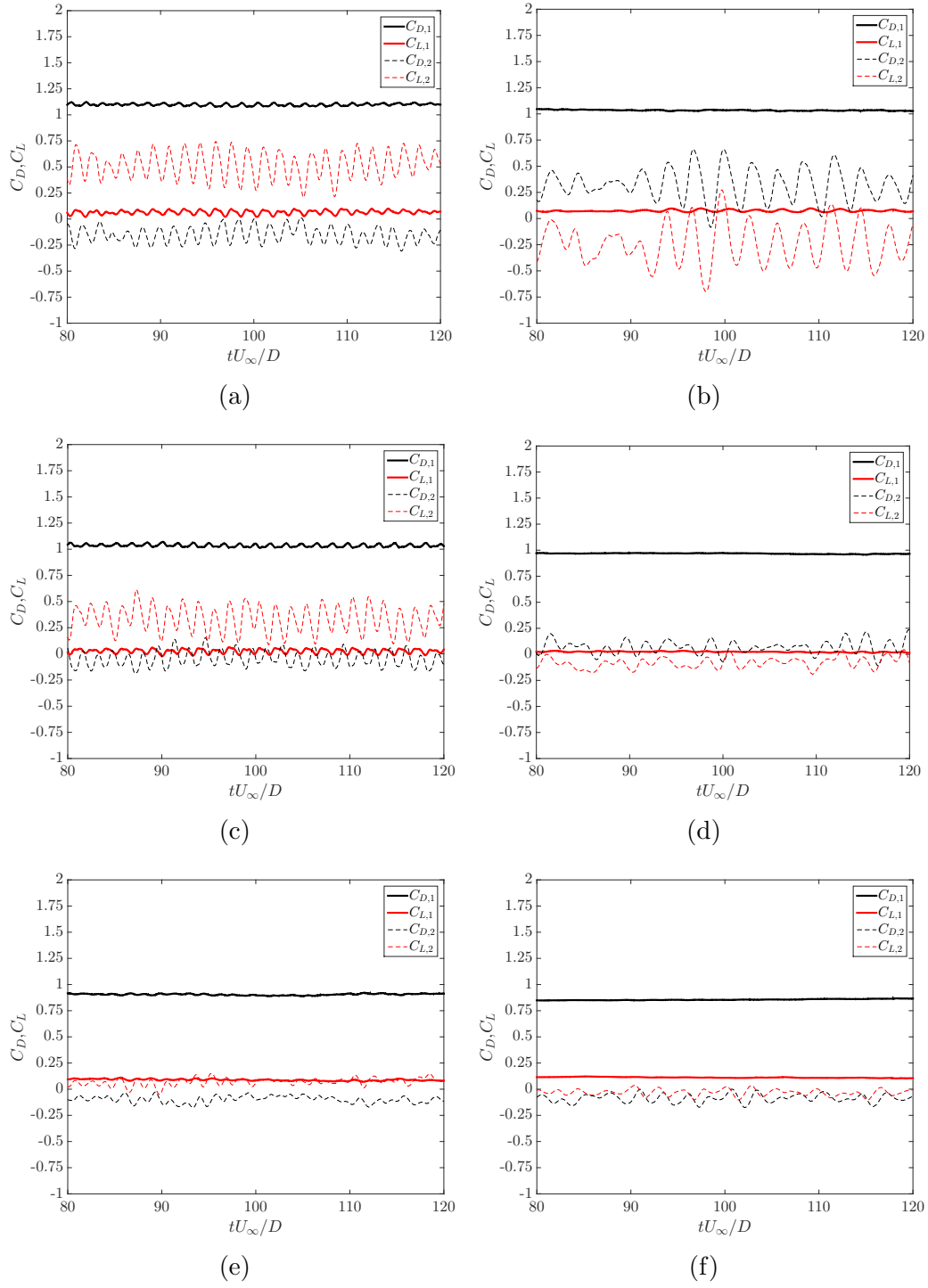
Figure 4. Time histories of C_L and C_D of both upstream and downstream cylinders: (a) $L/D = 2$, $G/D = 0.5$ (b) $L/D = 5$, $G/D = 0.5$ (c) $L/D = 2$, $G/D = 0.3$ (d) $L/D = 5$, $G/D = 0.3$ (e) $L/D = 2$, $G/D = 0.1$ (f) $L/D = 5$, $G/D = 0.1$.

15

data in Wang et al. (2015) [29] when G/D is small. However, the present results deviate from their experimental data for relatively larger G/D. This is possibly attributed to two factors. Firstly, when the gap is small the vortex shedding is very much suppressed, whereas the wake is completely turbulent and chaotic for relatively larger G/D which induces uncertainties for the flow which the downstream cylinder is subjected to. Secondly, the present numerical study and the reference experimental study are conducted at different Re, which may also give rise to the discrepancy. Therefore, although the trend of RMS force coefficients is captured, the values deviate from the experimental data for the downstream cylinder for the cases of relatively large G/D.

4.2   Flow Field

After discussing how the gap ratio and the pitch ratio affect the hydrodynamic force coefficients, the focus is to investigate the flow field in this section. The flow field for all six simulated cases is discussed from two perspectives: the mean flow and the instantaneous flow characteristics.

4.2.1   Mean Flow Characteristics

The time- and spanwise-averaged streamwise velocity in the cylinders' wake normalized by the free stream velocity, u_{mean}/U_∞, at cylinders' centerlines ($y = G + 0.5D$) are illustrated in Figure 7 for both pitch ratios. The cylinder wake can be characterised by the recirculation length, L_r, defined as the distance between the cylinder base and the point of zero streamwise mean velocity. To clearly identify mean flow characteristics, Figures 8 and 9 depict the time-averaged streamlines at the cylinder spanwise mid-plane ($z/D = 2$) for $L/D = 2$ and 5 with the background of time-averaged pressure field, respectively. Here, the time-averaged pressure is the mean pressure calculated for the quasi-steady time period.

As displayed in Figure 7a, there are no conspicuous zero-crossings of the streamwise velocity between the two cylinders at $L/D = 2$. In the wake of the downstream cylinder, L_r is similar for $G/D = 0.5$ and 0.3, but much smaller than that of the smallest gap ratio, $G/D = 0.1$. The reason for this is that the recirculation mechanism for $G/D = 0.1$ is different from $G/D = 0.5$ and 0.3. It is shown in Figures 8a and 8b that, at $G/D = 0.5$ and 0.3, the well defined recirculation zone behind the downstream cylinder is caused by vortex shedding, while the vortex shedding is strongly suppressed at $G/D = 0.1$ as shown in Figure 8c. In the experiments of Wang and Tan (2008) [43], they reported a similar trend for a single cylinder in the vicinity of a plane wall and concluded that the recirculation length increases with the decrease in the gap
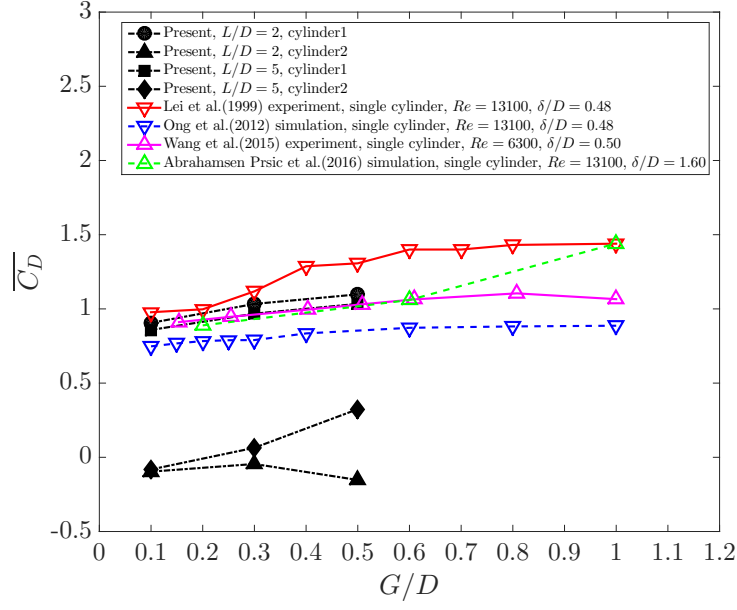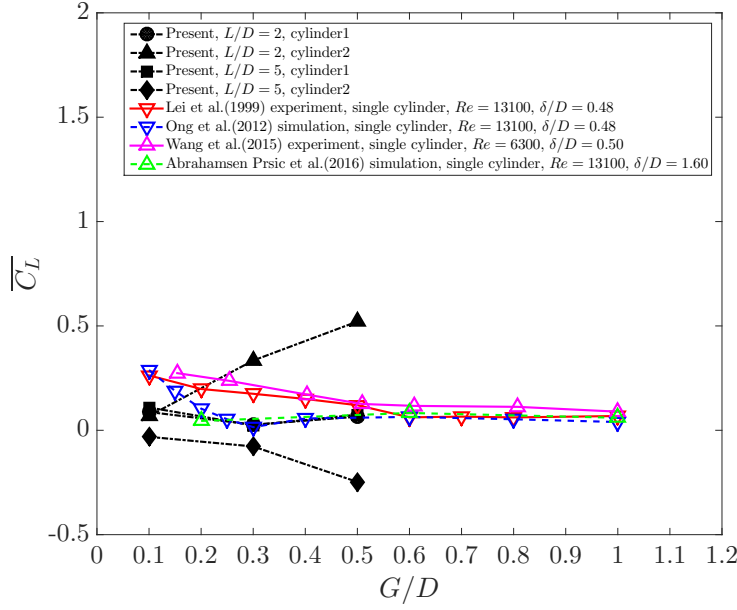
Figure 5. Mean force coefficients of both the upstream and the downstream cylinders as a function of G/D: (a) $\overline{C_D}$ (b) $\overline{C_L}$.

ratio. Since $L/D = 2$ is considered in the reattachment regime in the present study, L_r is seen to follow the same trend in the wake of the downstream cylinder. The reason why $L/D = 2$ is classified in the reattachment regime will be discussed in Section 4.2.2. After the recirculation zone, u_{mean}/U_∞ is largest at the largest gap ratio of $G/D = 0.5$ among the three cases.
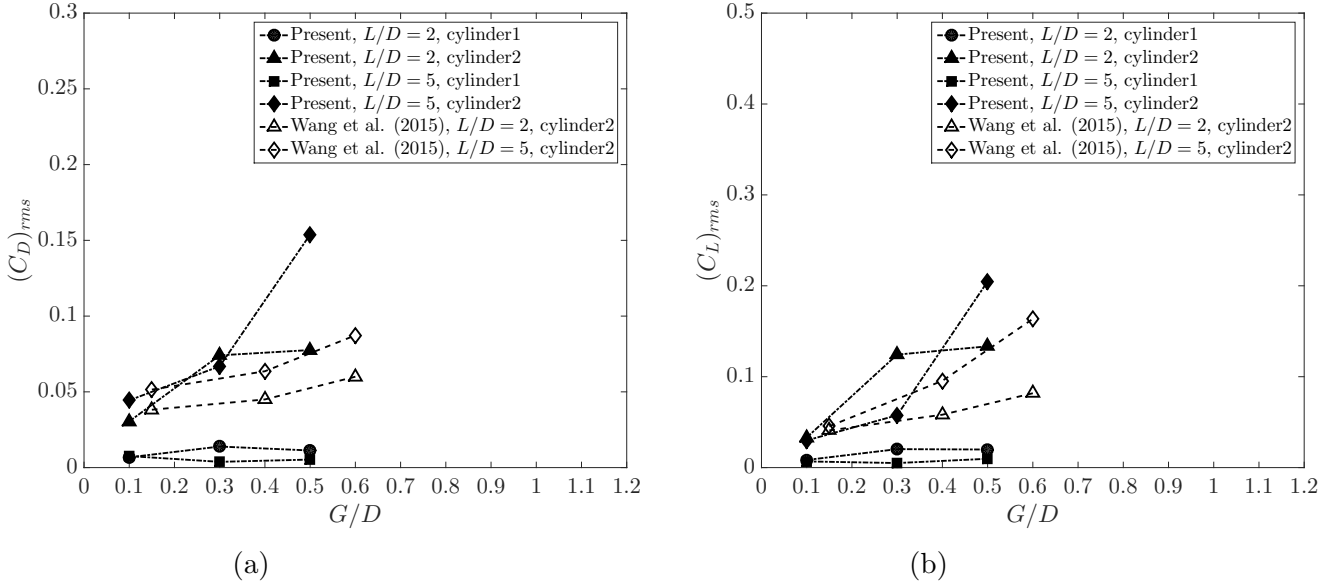
Figure 6. RMS force coefficients of both the upstream and the downstream cylinders as a function of G/D: (a) $(C_D)_{rms}$ (b) $(C_L)_{rms}$.

The observation is different for the case of $L/D = 5$, as shown in Figure 7b. Given a much larger space between the tandem cylinders, the recirculation is clearly formed in the wake of the upstream cylinder at $G/D = 0.5$ and 0.3. L_r for $G/D = 0.5$ is slightly larger than that of $G/D = 0.3$. At $G/D = 0.1$, the recirculation cannot be clearly defined as the mean streamwise velocity crosses the zero-line multiple times. As for the wake of the downstream cylinder, L_r for $G/D = 0.5$ is larger than those of $G/D = 0.3$ and 0.1. This is attributed to the fact that the recirculation mechanism for $G/D = 0.5$ is different from those for $G/D = 0.3$ and 0.1. It is observed in Figure 9a that, at $G/D = 0.5$, a well-defined recirculation zone behind the downstream cylinder is caused by vortex shedding. However, the vortex shedding becomes suppressed at $G/D = 0.3$ and 0.1, as shown in Figures 9b and 9c, respectively. Similarly for the case of $L/D = 2$, behind the recirculation zones of both cylinders, u_{mean}/U_∞ is the largest at the largest gap ratio of $G/D = 0.5$ among the three cases.

For $L/D = 2$, in the cases of $G/D = 0.5$ and 0.3, as shown by Figures 8a and 8b, the most noticeable feature is the squarish cavity-like flow formed between the two cylinders. This means that most part of the flow between the tandem cylinders circulates in the cavity and is trapped in between the cylinders in the time averaging sense. Above the primary recirculation cavity, there exists a secondary, small recirculation zone. This secondary recirculation zone vanishes at $G/D = 0.1$, as shown in Figure 8c. This is because such a small gap ratio deflects the primary recirculation zone upwards away from the wall. As a result, the secondary recirculation zone is pushed out of the space between the cylinders and convected by the free stream. At all gap ratios, two small recirculations can also be observed on the bottom wall at locations

slightly in front of both cylinders, i.e. approximately at $8 < x/D < 9$ and $11 < x/D < 12$. As G/D decreases, these two recirculations become more pronounced. This is attributed to the fact that the bottom wall boundary layer is separated due to the existence of the cylinders and the formation of the adverse pressure gradient. This eventually leads to a recirculation at two specific locations on the bottom wall. It is also worth noting that, in Figure 8c, a large lee-wake vortex is formed behind the downstream cylinder. In ocean engineering applications, this lee-wake recirculation vortex is of significant importance in scouring of the subsea pipelines laid on or in proximity to the seabed, as shown in the works of Brørs (1999) [44] and Li and Cheng (2001) [45]. In the time averaging sense, the flow is recirculating over a long streamwise distance behind the downstream cylinder because of the dominant adverse pressure. Slightly in front of the primary recirculation zone, a small secondary recirculation zone is observed just next to the downstream cylinder.

For the cases of $L/D = 5$, as shown in Figure 9, the flow field behaves very differently as compared to $L/D = 2$. In Figure 9a, at $G/D = 0.5$, a larger pitch ratio allows the flow behind the upstream cylinder to form a nearly symmetric recirculation cavity-like flow deflected away from the wall. It is conspicuous that the bottom wall boundary layer is very much disturbed at around $12 < x/D < 14$, forming a pronounced recirculation zone. This recirculation zone becomes increasingly stronger as G/D becomes smaller. Figure 9b represents an intermediate state between $G/D = 0.5$ and $G/D = 0.1$. In the extreme case, at $G/D = 0.1$, shown in Figure 9c, the recirculation transforms to a rectangular cavity-like flow which resembles the one seen in Figure 8a. The length of the lee-wake recirculation for $L/D = 5$ with $G/D = 0.1$ is considerably shorter than the case of $L/D = 2$ and $G/D = 0.1$ as displayed in Figure 8c. The reason for this is that the effective streamwise length of the bluff body of $L/D = 2$, which is in the range of the reattachment regime, is larger than that of $L/D = 5$, which falls in the range of the co-shedding regime. A larger effective streamwise length of the bluff body subjected to the incoming flow leads to a larger lee-wake recirculation zone.

To sum up, by investigating the normalized time- and spanwise-averaged streamwise velocity profile in Figure 7 and the time-averaged streamlines at the cylinder spanwise mid-plane in Figures 8 and 9, it clearly shows that the gap ratio and pitch ratio greatly affect the flow field in a time averaging sense.

Further, Figure 10 shows the mean pressure coefficient, C_p, around the mid-plane of the cylinders to study the force distribution on the structure. Here, the pressure coefficient, C_p, is defined as

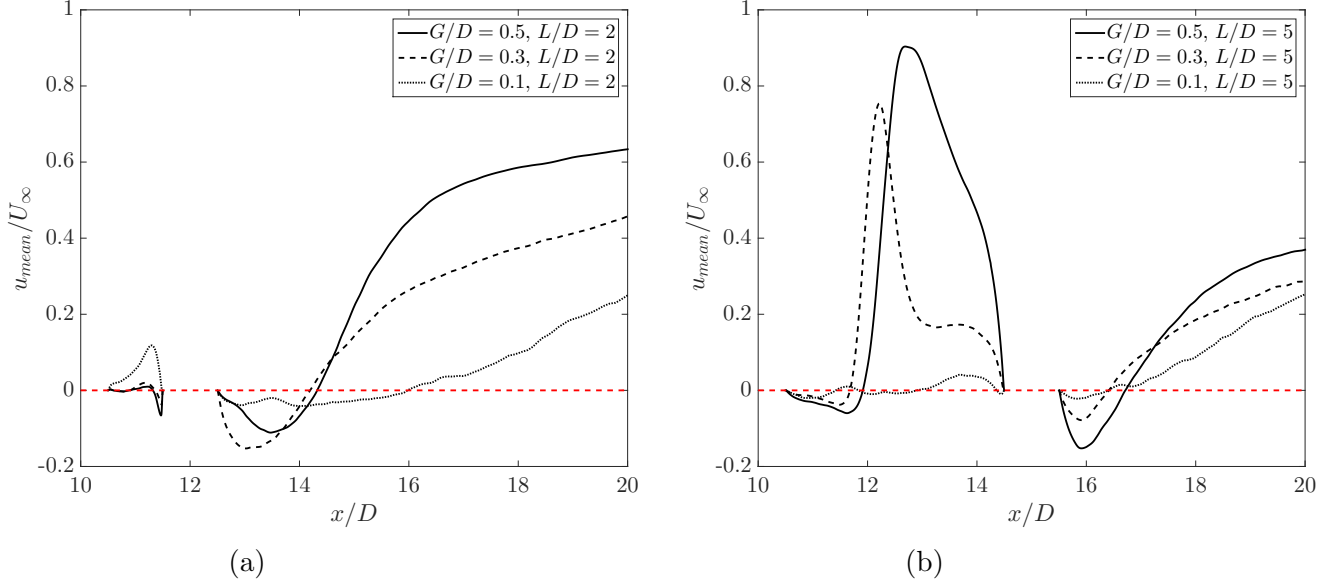$$C_p = \frac{p - p_\infty}{\frac{1}{2}\rho U_\infty}, \tag{13}$$

19

Figure 7. Normalized time- and spanwise-averaged streamwise velocity profiles for different G/D: (a) $L/D = 2$, (b) $L/D = 5$.

where p_∞ is taken as the mean pressure at the inlet mid-plane over the crossflow direction from $(0D, G, 2D)$ to $(0D, G + D, 2D)$. For instance, at $G/D = 0.5$, p_∞ is the time-averaged pressure over the vertical distance from $(0D, 0.5D, 2D)$ to $(0D, 1.5D, 2D)$. p denotes the mean pressure (i.e. time-averaged pressure over the quasi-steady time period) at the peripheral angle of the cylinder, θ, measured clockwise from the point on the frontal surface.

C_p distributions around the upstream cylinder for $L/D = 2$ and 5 are compared with the experimental data in Lei et al. (1999) [34] for the flow past a single cylinder placed in the vicinity of a plane wall at $G/D = 0.6$, 0.4 and 0.1 with $\delta/D = 0.48$ and $Re = 1.31 \times 10^4$, as shown in Figures 10a and 10c. At both pitch ratios, for $G/D = 0.5$ and 0.3, C_p distribution agrees quite well with the experimental results at $G/D = 0.6$ and 0.4, respectively. However, at $G/D = 0.1$, the present results deviate from the reference data in the region around the lower frontal surface of the upstream cylinder $(270° < \theta < 360°)$. The discrepancy might be attributed to the fact that though the same boundary layer thickness of $\delta/D = 0.48$ has been used in our numerical study and the experimental study, the wall boundary layer might have obtained a structure somewhat different from the logarithmic profile in the experiments. Generally, the present simulation results have captured the same trend as the experimental data. In the present study, at both pitch ratios, C_p distributions around the mid-plane of the upstream cylinder at $G/D = 0.5$ and 0.3 are almost symmetric about the horizontal centerline of the cylinder. However, at $G/D = 0.1$ the narrow gap skews the distribution and C_p becomes asymmetric to a large extent due to the strong wall proximity interference.

20

Figure 8. Time-averaged flow streamlines at spanwise mid-plane with time-averaged pressure field for $L/D = 2$: (a) $G/D = 0.5$, (b) $G/D = 0.3$, and (c) $G/D = 0.1$ for flow coming from left to right.

In Figures 10b and 10d, C_p distributions around the downstream cylinders at both pitch ratios are presented. The most striking observation is that, at $L/D = 2$ in the reattachment regime, C_p distribution is skewed downwards to the bottom plane wall, providing a positive lift component; whereas, C_p distribution is skewed upwards away from the bottom plane wall at $L/D = 5$ in the co-shedding regime, providing a negative lift component. The skewness of the stagnation point of the downstream cylinder is consistent with Figure 5b which shows that $\overline{C_{L,2}} > 0$ for $L/D = 2$ and $\overline{C_{L,2}} < 0$ for $L/D = 5$. This can be explained by the earlier observation seen in the time-averaged streamlines

21

Figure 9. Time-averaged flow streamlines at spanwise mid-plane with time-averaged pressure field for $L/D = 5$: (a) $G/D = 0.5$, (b) $G/D = 0.3$, and (c) $G/D = 0.1$ for flow coming from left to right.

shown in Figures 8 and 9. For the case of $L/D = 2$, the cavity-like flow formed via the shear layer reattachment in between the tandem cylinders is skewed upwards with respect to the centerline of the downstream cylinder leading to a region with relatively high pressure at the frontal lower surface of the downstream cylinder, i.e. $270° < \theta < 360°$. This leads to a higher C_p at this particular quadrant, which is evidenced in Figure 10b. However, at $L/D = 5$, the mechanism of forming the recirculation zone is totally different as compared to $L/D = 2$. The recirculation zone is developed from the separated bottom wall boundary layer, and this gives rise to a higher pressure region on

the frontal upper surface of the downstream cylinder, i.e. $0° < \theta < 90°$. This higher C_p distribution at this particular quadrant is recorded in Figure 10d.

It is also worth plotting the maximum C_p around the cylinder, $(C_p)_{max}$, as a function of G/D for both the upstream and the downstream cylinders at both pitch ratios. In Figure 11a, it is apparent that $(C_p)_{max}$ decreases as G/D decreases. The curves of $(C_p)_{max}$ of the upstream cylinder at $L/D = 2$ and 5 almost coincide as the frontal surface of the upstream cylinder is subjected to almost the same flow conditions for both pitch ratios. As for the downstream cylinder, a smaller pitch ratio leads to a higher $(C_p)_{max}$. The variation of the front stagnation point, θ_{stag}, as a function of G/D, is presented in Figure 11b. Here, the stagnation point, θ_{stag}, is determined as the front symmetry point of the zero crossings of the pressure distribution, according to Surry (1972) [46]. Note that for cases of the downstream cylinder at $L/D = 2, G/D = 0.1$ and at $L/D = 5, G/D = 0.3$ and 0.1, there is no zero crossing since $C_p < 0$ for all θ. Thus, in these cases, θ_{stag} is determined as the location at which C_p is maximum. For ease of presentation, θ_{stag} is taken as $\theta_{stag} = \theta - 360°$ if $\theta \in [270°, 360°]$ in Figure 11b. It is shown that the stagnation point moves upwards with respect to the cylinder centerline on the frontal surface of both the upstream and the downstream cylinders as G/D becomes smaller in all cases.

4.2.2 Instantaneous Flow Characteristics

While the general flow features can be discussed by studying the force coefficients and the time-averaged streamlines in the earlier section, the more specific details of the flow can be further investigated via the instantaneous flow fields. In the following, the isosurfaces of spanwise vorticity, ω_z, streamwise vorticity, ω_x, are illustrated to further analyse the flow details.

Figures 12 and 13 depict the instantaneous isosurfaces of ω_z ($-40 \leq \omega_z \leq 40$) and ω_x ($-40 \leq \omega_x \leq 40$) for $L/D = 2$ with different gap ratios, respectively. In Figures 12a, 12b and 12c, the common characteristic at these three gap ratios is that the boundary layer developed on the upstream cylinder is still laminar, yielding an almost two-dimensional wake, while the wake behind the downstream cylinder is largely turbulent. This is consistent with the fact that at $Re = 1.31 \times 10^4$, in the subcritical regime, the boundary layer remains laminar and the wake becomes turbulent, according to Sumer and Fredsøe (2010) [3]. Another interesting feature is that the bottom shear layer from the upstream cylinder reattaches to the surface of the downstream cylinder. This is the reason we classify this pitch ratio of $L/D = 2$ in the reattachment regime. At this particular pitch ratio, the cylinders are placed sufficiently far apart that the shear layers from the upstream cylinder can no longer enclose the downstream cylinder but rather reattach onto the downstream cylinder.
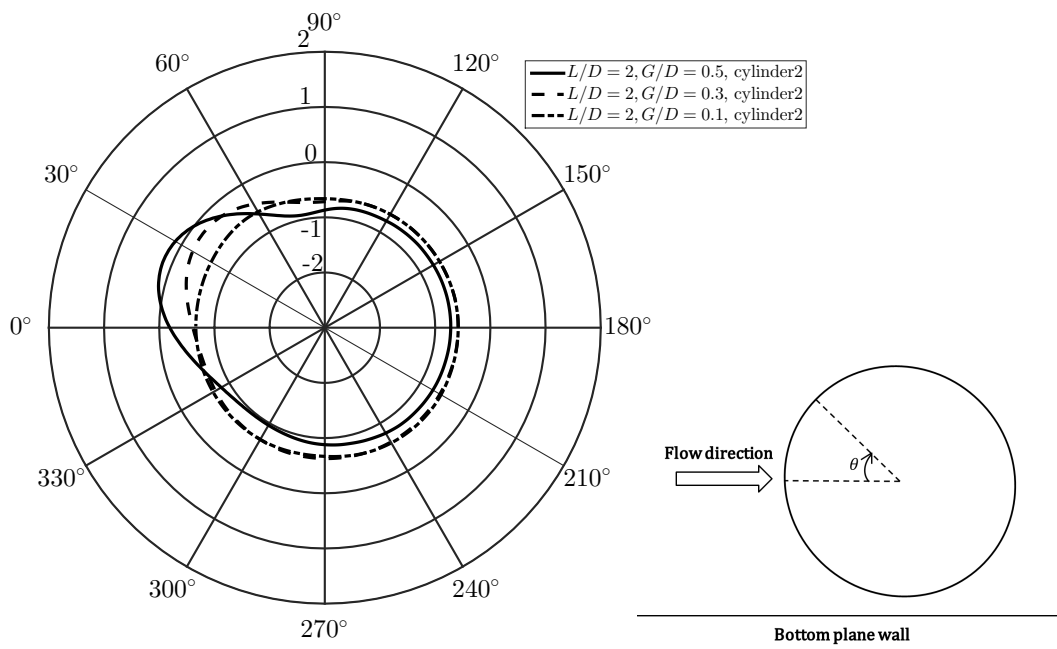
(a)

(b)

24
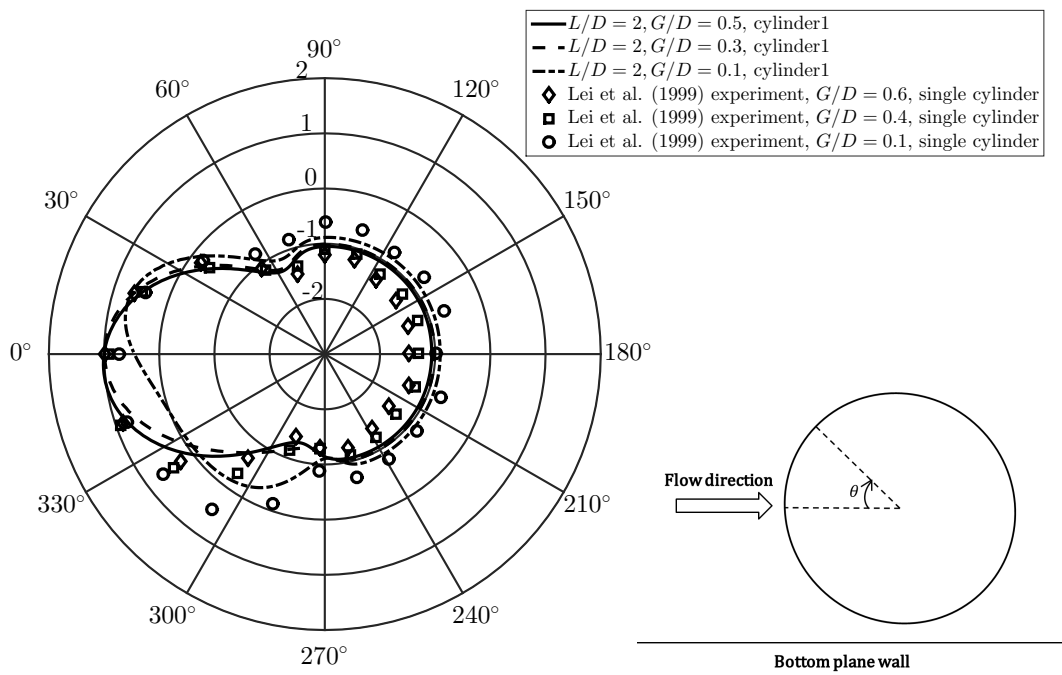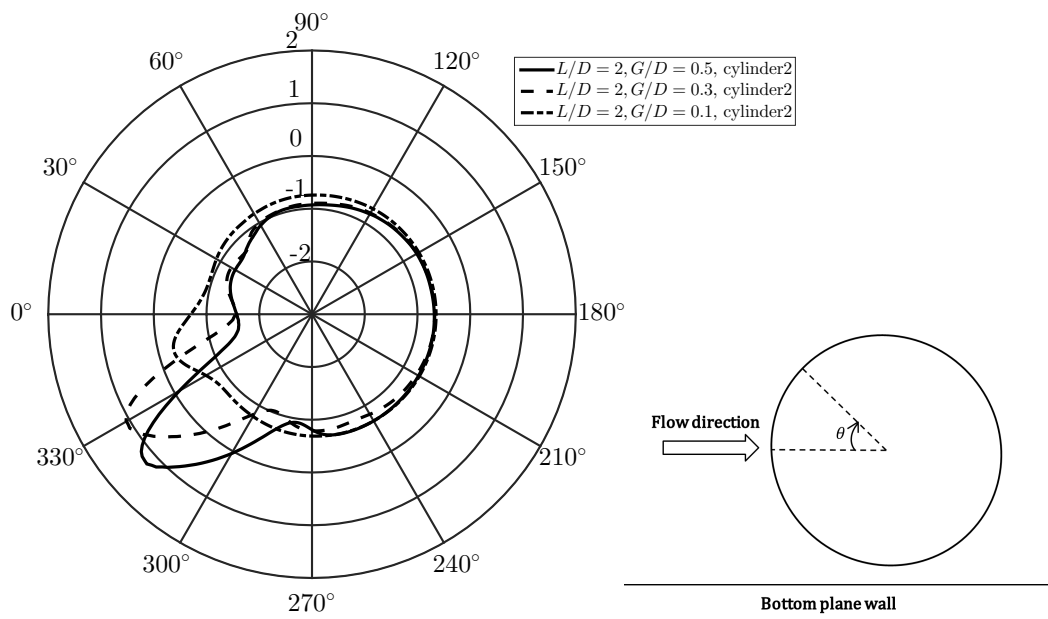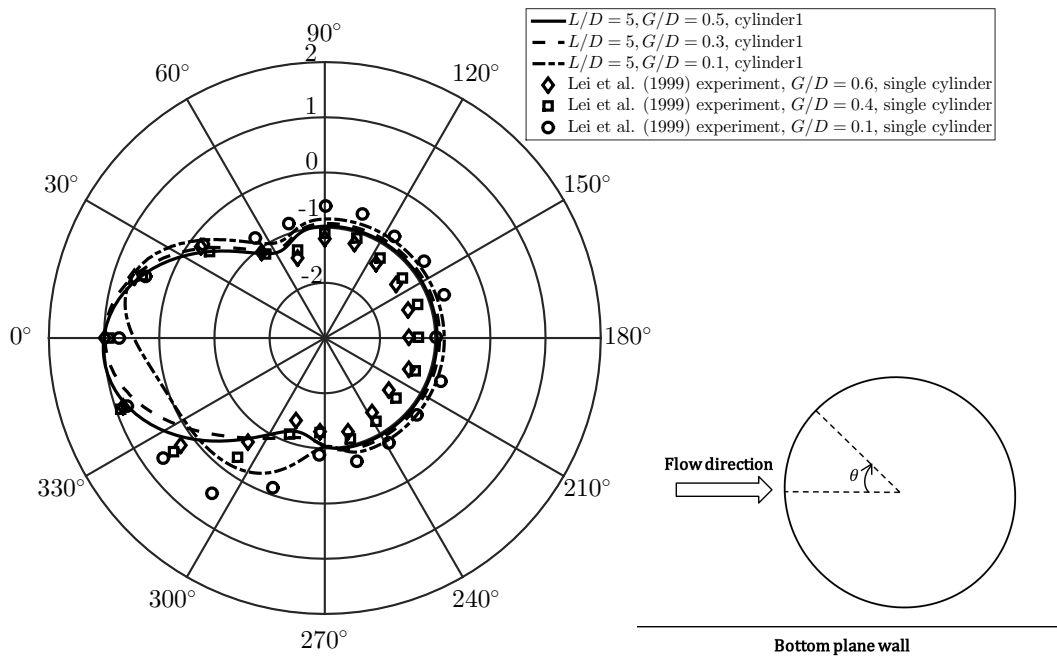
(c)

(d)

Figure 10. Mean pressure coefficient around the cylinder mid-plane: (a) upstream cylinder at $L/D = 2$, (b) downstream cylinder at $L/D = 2$, (c) upstream cylinder at $L/D = 5$, and (d) downstream cylinder at $L/D = 5$.
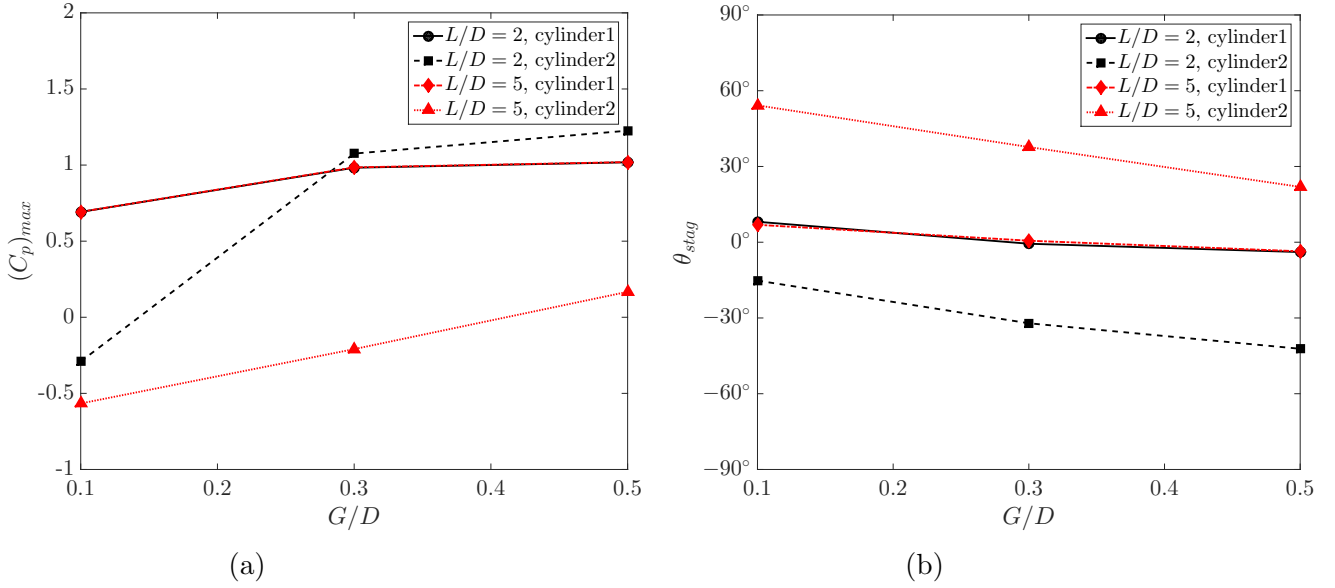
25

Figure 11. (a) Maximum mean pressure coefficient $(C_p)_{max}$, (b) Stagnation point θ_{stag} as a function of G/D at both pitch ratios for both the upstream and the downstream cylinders.

Igarashi et al. (1981) [10] showed that at smaller pitch ratios ($1.1 < L/D < 1.6$) in the reattachment regime the shear layers form the upstream cylinder alternatingly attach onto the front face of the downstream cylinder, and the reattachment process is synchronized with Kármán vortex shedding from the downstream cylinder. However, in the present study, Figures 12a and 12b illustrate that, at $G/D = 0.5$ and 0.3, the bottom shear layer from the upstream cylinder reattaches onto the front surface of the downstream cylinder because of the influence of the neighbouring wall. The reattachment of the shear layer is only established on the bottom half of the upstream cylinder due to the deflection away from the wall. This biased reattachment process forms the cavity-like recirculation zone, observed in Figures 8a and 8b. At $G/D = 0.1$, the bottom shear layer from the upstream cylinder is strongly suppressed and weakened so the biased reattachment is not as conspicuous as at $G/D = 0.5$ and 0.3. Igarashi (1981) [10] also showed that, at intermediate pitch ratios within the reattachment regime ($1.6 < L/D < 2.3 - 2.4$), the shear layer reattachment is nearly continuous and a pair of quasi-stationary eddies forms in the gap. Alam et al. (2003) [16] also reported steady attachment of the shear layers on the downstream cylinder at $Re = 6.5 \times 10^4$. Zhou and Yiu (2006) [13] noted that, for $L/D = 2 - 3$, the shear layer reattachment occurs more often on the downstream side of the second cylinder. It interferes with the boundary layer development and the separation on the downstream cylinder, and the Kármán vortices formed behind the downstream cylinder are relatively weak and small. Such relatively weak vortices from the downstream cylinder seen in Figure 12 are consistent with the observation in Zhou and Yiu (2006) [13].

The cavity-like flow is formed between the cylinders at $L/D = 2$, while the vortex formation of the upstream cylinder is not disturbed to a large extent due to the presence of the bottom plane wall but rather due to the presence of the downstream cylinder. For experimental studies on flow around wall-free tandem cylinders, the same characteristics of the wake flow are captured in the smoke wind tunnel experiments by Igarashi (1981) [10] at $Re = 1.3 \times 10^4$ and Ljungkrona and Sundén (1993) [47] at $Re = 1.2 \times 10^4$. Due to the nature of the measurements, these experimental results were not capable of describing the fine structures and the complex dynamics in the space between two cylinders and in the near wake and in the gap between the cylinder bottom and the plane wall. The present study therefore complements the experimental conclusions.

It is apparent to note that the counter-clockwise vortices in the near wake of the downstream cylinder become weaker as G/D decreases from 0.5 to 0.1 since the cylinder bottom shear layer roll-up gets strongly suppressed by the neighbouring wall. Li et al. (2016) [48] discussed the detailed mechanism involved in the vortex suppression in the process of vortex-induced vibrations (VIV) of an elastically mounted cylinder in the vicinity of a plane wall at $Re = 200$. They observed that the counter-clockwise vortices shed from the cylinder bottom force the plane wall boundary layer to separate and induce secondary clockwise vortices. Those induced secondary vortices eventually coalesce with the clockwise vortices shed from the cylinder top surface. The merging process strongly suppresses the development of the clockwise vorticity shed from the cylinder bottom. This mechanism can also be applied here, in Figure 12, that the vortices shed from the downstream cylinder bottom are weakened by the decreasing G/D.

Figure 13 displays how the wall proximity influences the isosurfaces of ω_x in flow past two near-wall cylinders in tandem for $L/D = 2$. As G/D decreases from 0.5 to 0.1, ω_x from the cylinder top is convected longer distance from the downstream cylinder. However, ω_x becomes more suppressed from the bottom surface of the downstream cylinder and gradually weakens as G/D decreases. At $G/D = 0.1$, ω_x from the bottom downstream cylinder almost vanishes, as shown in Figure 13c. It is also worth noting that stronger ω_x or more spanwise variation is found in the space between the two cylinders as G/D decreases.

Figures 14 and 15 depict the instantaneous isosurfaces of ω_z ($-40 \leq \omega_z \leq 40$) and ω_x ($-40 \leq \omega_x \leq 40$) for $L/D = 5$ with different gap ratios, respectively. At $L/D = 5$, ω_z and ω_x behave very differently as compared to $L/D = 2$. In Figure 14, the most striking feature is that the downstream cylinder is sufficiently far away so that Kármán vortex shedding can occur from the upstream cylinder. The downstream cylinder is located outside the vortex formation region of the upstream cylinder and experiences the periodic impingement of Kármán vortices shed from the upstream cylinder. Zdravkovich (1987) [9] and Zhou and Yiu (2006) [13] pointed out that this happens at approximately
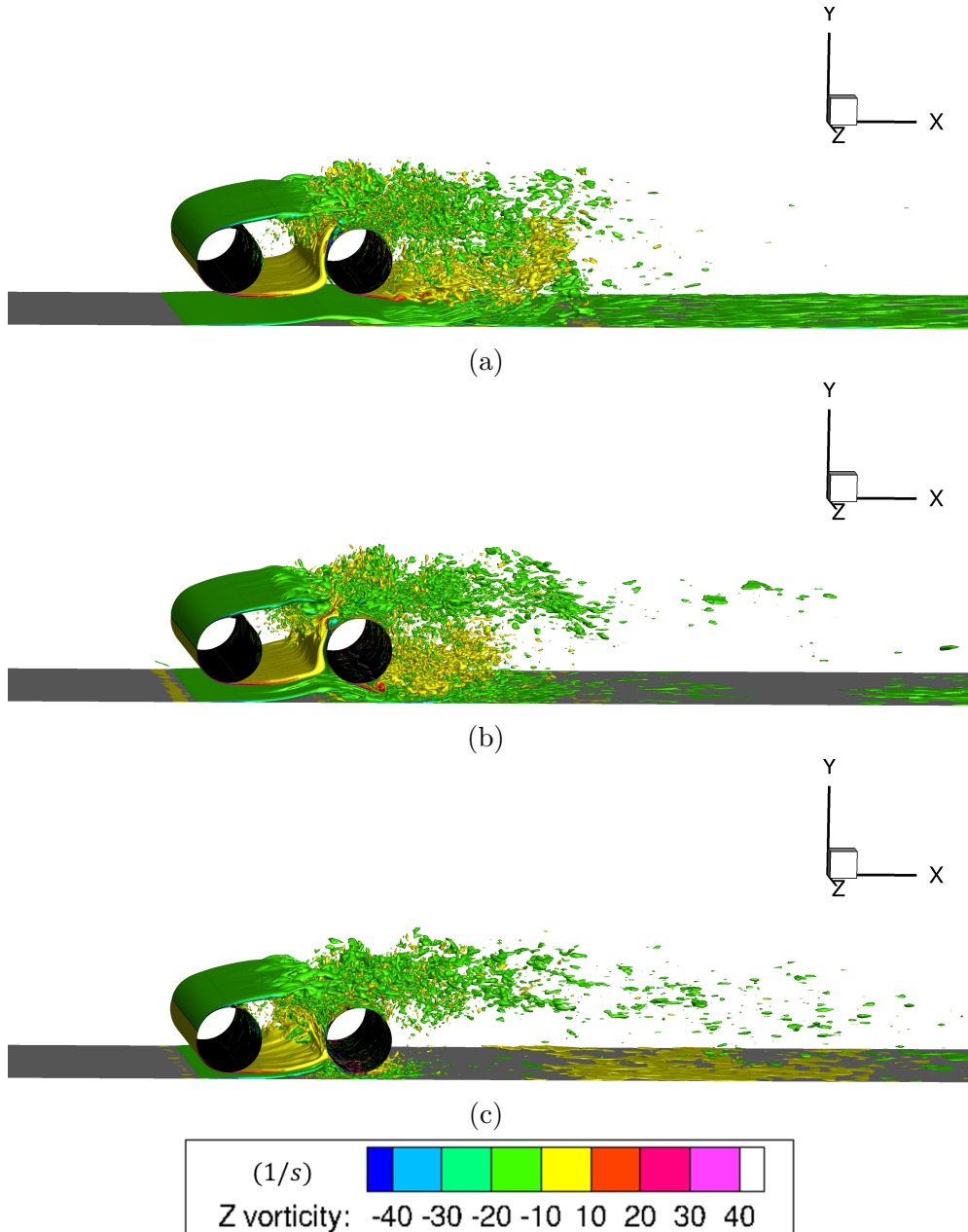
Figure 12. Instantaneous isosurfaces of spanwise vorticity, ω_z, for $L/D = 2$: (a) $G/D = 0.5$, (b) $G/D = 0.3$, and (c) $G/D = 0.1$ for the flow coming from left to right.

$L/D > 3.4 - 3.8$ and $L/D > 5$, respectively.

In the numerical study of Meneghini et al. (2001) [20], the authors pointed out that the impingement results in an amalgamation process as vortices shed from the upstream cylinder merge with those forming from the downstream cylinder. This is consistent with the present findings. For instance, at $G/D = 0.5$, shown in Figure 14a, the incident vortices are severely distorted as they are swept around the downstream cylinder. Zhou and Yiu (2006) [13] found that,
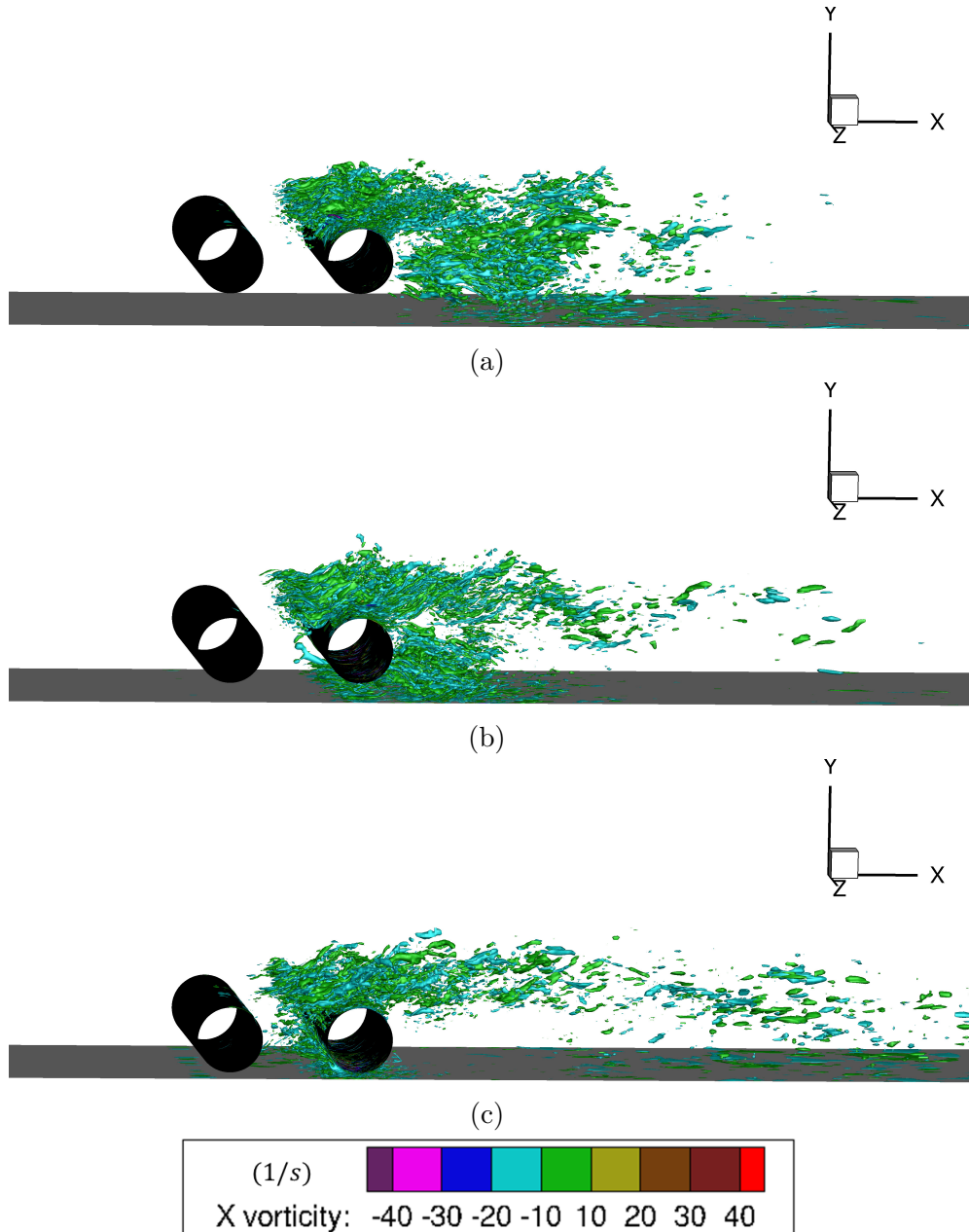
Figure 13. Instantaneous isosurfaces of streamwise vorticity, ω_x, for $L/D = 2$: (a) $G/D = 0.5$, (b) $G/D = 0.3$, and (c) $G/D = 0.1$ for the flow coming from left to right.

in the co-shedding regime, the resulting Kármán vortices shed from the downstream cylinder are weaker compared to those in the reattachment regime. This can be observed by comparing Figures 12a and 12b with Figures 14a and 14b, where the vortices shed from the downstream cylinder are weaker at $L/D = 5$ than $L/D = 2$. The shed vortices weaken and dissipate more quickly partially owing to the vortex impingement process. At the smallest gap ratio of $G/D = 0.1$, both pitch ratios give rise to very weak downstream vortices because of the strong vortex shedding suppression, observed in Figures 12c

29

and 14c.

Figure 15 illustrates how the wall proximity influences the isosurfaces of ω_x in flow past two near-wall cylinders in tandem for $L/D = 5$. ω_x becomes stronger in the near-wake of the upstream cylinder or more spanwise variation is noticed in the space between the tandem cylinders as G/D gets smaller. However, the intensity of ω_x in the near-wake of the downstream cylinder decreases with decreasing gap ratio since the streamwise vortices shed from cylinder bottom are also suppressed and weakened.
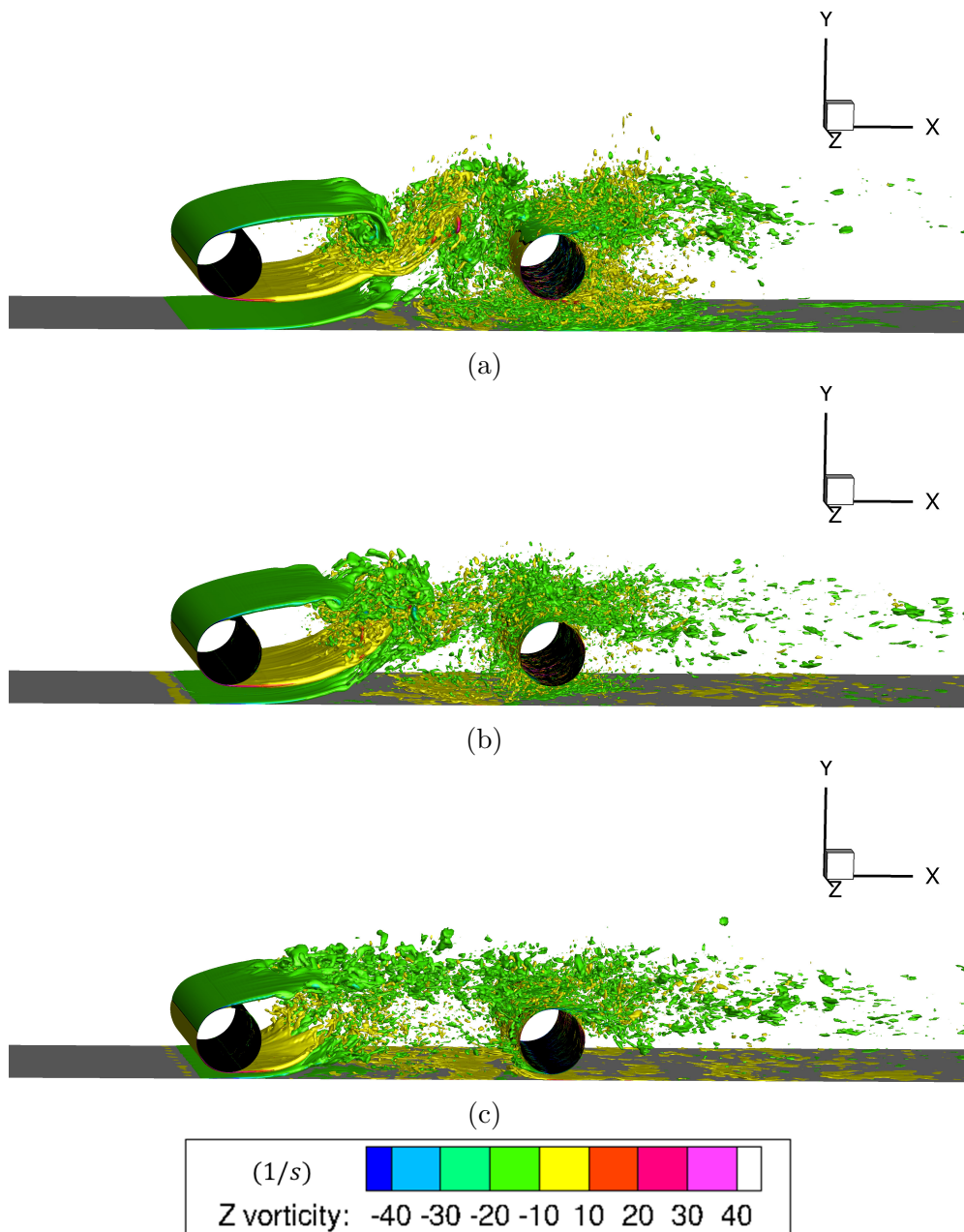
Figure 14. Instantaneous isosurfaces of spanwise vorticity, ω_z, for $L/D = 5$: (a) $G/D = 0.5$, (b) $G/D = 0.3$, and (c) $G/D = 0.1$ for the flow coming from left to right.
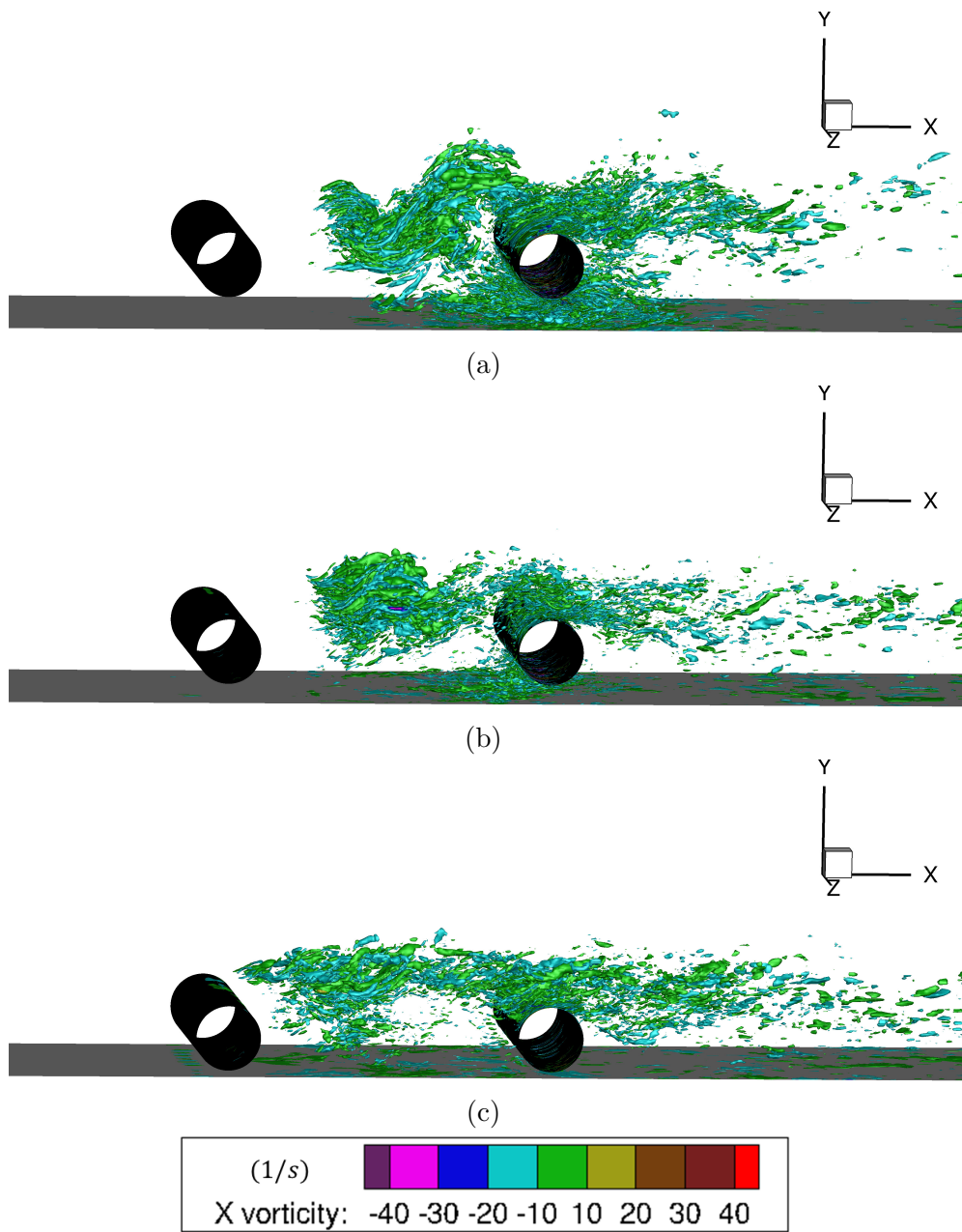
Figure 15. Instantaneous isosurfaces of streamwise vorticity, ω_x, for $L/D = 2$: (a) $G/D = 0.5$, (b) $G/D = 0.3$, and (c) $G/D = 0.1$ for the flow coming from left to right.

5 Concluding Remarks

Six combinations of different pitch ratios, L/D, and gap ratios, G/D, for the flow past two circular cylinders in proximity to a plane wall have been numerically simulated using Large Eddy Simulations (LES) with Smagorinsky subgrid scale model. The present study is basically divided into two parts: mean and instantaneous flow characteristics.

The major findings regarding the mean flow characteristics are as follows. (1) With both pitch ratios, the wall proximity has a decreasing effect on the mean drag coefficient of the upstream cylinder, $\overline{C_{D,1}}$. (2) At $L/D = 2$, in the reattachment regime, the mean drag coefficient of the downstream cylinder, $\overline{C_{D,2}}$, is negative since it is located within the drag inversion separation distance. On the other hand, at $L/D = 5$, in the co-shedding regime, $\overline{C_{D,2}} < 0$ at $G/D = 0.1$ but increases to the positive range at $G/D = 0.3$ and 0.5. (3) The mean lift coefficient of the downstream cylinder, $\overline{C_{L,2}}$, $\overline{C_{L,2}}$ increases with the increase of G/D for $L/D = 2$, while an inverse trend is observed for $L/D = 5$. (4) In terms of the time-averaged flow fields, at $L/D = 2$, there exists a cavity-like flow between the tandem cylinders and flow circulates within the cavity. A long lee-wake recirculation zone is found behind the downstream cylinder at $G/D = 0.1$. However, a much smaller lee-wake recirculation zone is noticed behind the downstream cylinder at $L/D = 5$ with $G/D = 0.1$. (5) The stagnation point moves upwards with respect to the cylinder centerline on the frontal surface of both upstream and downstream cylinders as G/D becomes smaller.

While the overall flow features are discussed using the force coefficients and time-averaged flow characteristics, studying the instantaneous flow fields via vorticity distribution provides a detailed insight. Major conclusions can be drawn from the instantaneous flow characteristics are as follows. (1) At $L/D = 2$, the reattachment is biased to the bottom shear layer due to the deflection of the flow from the plane wall. This leads to the formation of the slanted squarish cavity-like recirculation zone in which the flow circulates between the tandem cylinders. (2) At both pitch ratios, as G/D narrows, stronger streamwise vortices, ω_x, are found between the two cylinders and vortices of less intensity are observed in the near wake of the downstream cylinder owing to the vortex shedding suppression of the neighbouring wall.

The present results have shown that our numerical implementation is capable of simulating the flow around two cylinders in tandem placed in close proximity to a plane wall with high fidelity. However, more experimental data are required to perform a more detailed validation study. In the meantime, the present study should be useful as an engineering assessment tool to estimate the hydrodynamic quantities and visualize the flow field for the case of sea

currents past two tandem subsea pipelines in the vicinity of the seabed in offshore applications.

Acknowledgement

References

[1] M. Abrahamsen Prsic, M.C. Ong, B. Pettersen, and D. Myrhaug. Large eddy simulations of flow around tandem cylinders close to a horizontal wall. *International Journal of Offshore and Polar Engineering*, 25:161–169, 2015.

[2] M.M. Zdravkovich. *Flow around circular cylinders, Vol.1: Fundamentals.* Oxford University Press, Oxford, UK, 1997.

[3] B.M. Sumer and J. Fredsøe. *Hydrodynamics around cylinderical structures. Revised, reprinted edition.* World Scientific Publishing, Singapore, 2010.

[4] A. Thom. An investigation of fluid flow in two-dimensions. *Aeronautical Research Council, Reports & Memoranda 1194*, 1928.

[5] P. Parnaudeau, J. Carlier, D. Heitz, and E. Lamballais. Experimental and numerical studies of the flow over a circular cylinder at Reynolds number 3900. *Physics of Fluids*, 20(085101), 2008.

[6] D.A. Lysenko, I.E. Ertesvåg, and K.E. Rian. Large-eddy simulation of the flow over a circular cylinder at Reynolds number 3900 using the openfoam toolbox. *Flow, Turbulence and Combust*, 89:491–518, 2012.

[7] M. Abrahamsen Prsic, M.C. Ong, B. Pettersen, and D. Myrhaug. Large-eddy simulations of three dimensional flow around a smooth circular cylinder in a uniform current in the subcritical flow regime. *Ocean Engineering*, 77:61–73, 2014.

[8] M.M. Zdravkovich. Flow induced oscillations of two interfering circular culinders. *Journal of Sound and Vibration*, 101:511–521, 1985.

[9] M.M. Zdravkovich. The effects of interference between circular cylinders in cross flow. *Journal of Fluids and Structures*, 1:239–261, 1987.

[10] T. Igarashi. Characteristics of the flow around two circular cylinders arranged in tandem (1st report). *Bulletin of the JSME*, 24:323–331, 1981.

[11] T. Igarashi. Characteristics of the flow around two circular cylinders arranged in tandem (2nd report, unique flow phenomenon at small spacing). *Bulletin of the JSME*, 27:2380–2387, 1984.

[12] S.J. Xu and Y. Zhou. Strouhal numbers in the wake of two inline cylinders. *Experiments in Fluids*, 37:248–256, 2004.

[13] Y. Zhou and M.W. Yiu. Flow structure, momentum and heat transport in a two-tandem-cylinder wake. *Journal of Fluid Mechanics*, 548:17–48, 2006.

[14] M.M. Zdravkovich and D.L. Pridden. Interference between two circular cylinders: series of unexpected discontinuities. *Journal of Industrial Aerodynamics*, 2:255–270, 1977.

[15] J.C. Lin, Y. Yang, and D. Rockwell. Flow past two cylinders in tandem: Instantaneous and average flow structure. *Journal of Fluids and Structures*, 16:1059–1071, 2002.

[16] M.M. Alam, M. Moriya, and K. Sakamoto. Fluctuating fluid forces acring on two circular cylinders in tandem arrangement at a subcritical Reynolds number. *Journal of Wind Engineering and Industrial Aerodynamics*, 91:139–154, 2003.

[17] F.-L. Song, S.-Y. Tseng, S.-W. Hsu, and C.-H. Kuo. Gap ratio effects on flow characteristics behind side-by-side cylinders of diameter ratio two. *Experimental. Thermal and Fluid Science*, 66:254–268, 2015.

[18] D. Sumner. Two circular cylinders in cross: A review. *Journal of Fluids and Structures*, 26:849–899, 2010.

[19] S. Mittal, V. Kumar, and A. Raghuvanshi. Unsteady incompressible flows past two cylinders in tandem and staggered arrangements. *International Journal of Numerical Methods in Fluids*, 25:1315–1344, 1997.

[20] J.R. Meneghini, F. Saltara, C.L.R. Siquiera, and J.R. Ferrari Jr. Numerical simulation of flow interference between two circular cylinders in tandem and side-byside arrangement. *Journal of Fluids and Structures*, 15:327–350, 2001.

[21] B.S. Carmo, J.R. Meneghini, and S.J. Sherwin. Secondary instabilities in the flow around two circular cylinders in tandem. *Journal of Fluid Mechanics*, 644:395431, 2010.

[22] T. Kitagawa and H. Ohta. Numerical investigation on flow around circular cylinders in tandem arrangement at a subcritical Reynolds number. *Journal of Fluid and Structures*, 24:680–699, 2008.

[23] A. Uzun and Y.M. Hussaini. An application of delayed detached eddy simulation to tandem culinder flow field prediction. *Computers and Fluids*, 60:71–85, 2012.

[24] H. Gopalan and R.K. Jaiman. Numerical study of the flow interference between tandem cylinders employing non-linear hybrid urans-les methods. *Journal of Wind Engineering and Industrial Aerodynamics*, 142:111–129, 2015.

[25] S. Taneda. Experimental investigation of vortex streets. *Journal of the Physical Society of Japan*, 20:1714–1721, 1998.

[26] S. Bhattacharyya and S. Dhinakaran. Vortex shedding in shear flow past tandem square cylinders in the vicinity of a plane wall. *Journal of Fluids and Structures*, 26:400–417, 2008.

[27] A.B. Harichandan and B. Roy. Vnumerical investigation of flow past single and tandem cylinderical bodies in the vicinity of a plane wall. *Journal of Fluids and Structures*, 33:19–43, 2012.

[28] A. Rao, M.C. Thompson, T. Leweke, and K. Hourigan. Dynamics and stability of the wake behind tandem cylinders sliding along a wall. *Journal of Fluid Mechanics*, 722:291–316, 2013.

[29] Wang X.K., J.-X. Zhang, Z. Hao, B. Zhou, and S.K. Tan. Influence of wall proximity on flow around two tandem circular cylinders. *Ocean Engineering*, 94:36–50, 2015.

[30] J.E. D'Souza, R.K. Jaiman, and C.K. Mak. Dynamics of tandem cylinders in the vicinity oif a plane moving wall. *Computers and Fluids*, 124:117–135, 2016.

[31] J. Smagorinsky. General circulation experiments with the primitive equations. *Monthly Weather Review*, 91:99–164, 1963.

[32] M. Abrahamsen Prsic, M.C. Ong, B. Pettersen, and D. Myrhaug. Large eddy simulations of flow around a circular cylinder close to a flat seabed. *Marine Structures*, 46:127–148, 2016.

[33] J.H. Ferziger and M. Peric. *Computational methods for fluid dynamics methods for fluid dynamics (3rd Ed)*. Springer-Verlag, Berlin, Germany, 2001.

[34] C. Lei, L. Cheng, and K. Kavanagh. Re-examination of the effect of a plane boundary on force and vortex shedding of a circular cyliner. *Journal of Wind Engineering*, 80:263–286, 1999.

[35] M.C. Ong, T. Utnes, L.E. Holmedal, D. Myrhaug, and B. Pettersen. Numerical simulation of flow around a circular cylinder close to a flat seabed at high Reynolds number using a $k - \epsilon$ model. *Coastal Engineering*, 57:931–947, 2010.

[36] A. Kravchenko and P. Moin. Numerical studies of flow over a circular cylinder at $Re = 3900$. *Physics of Fluids*, 12:403–417, 2000.

[37] J. Mathieu and J. Scott. *An introduction to turbulent flow*. Cambridge University Press, Cambridge, United Kingdom, 2000.

[38] S.B. Pope. *Turbulent flows*. Cambridge University Press, Cambridge, United Kingdom, 2000.

[39] B. Sainte-Rose, O. Allain, C. Leca, and A. Dervieux. A study of les models for the simulation of a turbulent flow around supercritical tandem cylinders. *Proceedings of the ASME 2014 33rd International Conference on Ocean, Offshore and Arctic Engineering (OMAE2014)*, (24031), 2014.

[40] P.W Bearman and M.M. Zdravkovich. Flow around a circular cylinder near a plane boundary. *Journal of Fluid Mechanics*, 89:33–47, 1978.

[41] M.M. Zdravkovich. *Flow around circular cylinders. vol.2: applications*. Oxford University Press, Oxford, United Kingdom, 2009.

[42] M.C. Ong, T. Utnes, L.E. Holmedal, D. Myrhaug, and B. Pettersen. Near-bed flow mechanisms around a circular marine pipeline close to a flat seabed in the subcritical regime using a $k - \epsilon$ model. *Journal of Offshore Mechanics and Arctic Engineering*, 134:021803, 2012.

[43] X.K. Wang and S.K. Tan. Comparison of flow patterns in the near wake of a circular cylinder and a square cylinder placed near a plane wall. *Ocean Engineering*, 35:458–472, 2008.

[44] B. Brørs. Numerical modelling of flow and scour at pipelines. *Journal of Hydraulic Engineering*, 125(5):511–523, 1999.

[45] F. Li and L. Cheng. Prediction of lee-wake scouring of pipelines in currents. *Journal of Waterway, Port, Coastal and Ocean Engineering*, 127:106–112, 2001.

[46] D. Surry. Some effects of intense turbulence on the aerodynamics of a circular cylinder at sub-critical Reynolds number. *Journal of Fluid Mechanics*, 52 (Part3):543–563, 1972.

[47] L. Ljungkrona and B. Sundén. Flow visualization and surface pressure measurement on two tubes in an inline arrangement. *Experimental, Thermal and Fluid Science*, 6:15–27, 1993.

[48] Z. Li, W. Yao, K. Yang, R.K. Jaiman, and B.C. Khoo. On the vortex-induced oscillations of a freely vibrating cylinder in the vicinity of a stationary plane wall. *Journal of Fluids and Structures*, 65:495–526, 2016.